Langmuir
Article
pubs.acs.org/Langmuir

Formation Process of Self-Assembled Monolayer on Gold Nanosphere Probed by Second Harmonic Generation

Tatsuya Yamaguchi,[†] Haruki Okawa,[‡] Kazuhiko Hashimoto,[‡] and Kotaro Kajikawa*,[†]

[†]*Interdisciplinary Graduate School of Science and Engineering, Tokyo Institute of Technology, 4259 Nagatsuta, Midori-ku, Yokohama 226-8502, Japan, and* [‡]*Department of Applied Chemistry, Faculty of Engineering, Kogakuin University, Nakano-cho, Hachioji, Tokyo 192-0015, Japan*

Received April 22, 2010. Revised Manuscript Received July 17, 2010

The formation process of a hemicyanine-terminated alkanethiolate self-assembled monolayer (SAM) on gold nanospheres immobilized on a glass substrate was studied by absorption spectroscopy, optical second harmonic generation, and Monte Carlo simulation. It was found that hemicyanine thiolate SAMs mainly form in the upper hemisphere region of the gold nanospheres in the early stage, followed by the additional SAM formation in the lower region of gold nanospheres. The hemicyanine SAM does not homogeneously form over the nanosphere surface and does not fully cover the nanospheres even after long exposure to the hemicyanine solution. This is because of the narrow space under the nanosphere, where the binding of the alkane disulfide to the gold surface is considered to be a diffusion-controlled reaction. The orientation of the hemicyanine molecules on gold nanospheres is similar to that of hemicyanine on a flat gold substrate. These results are important to understand the surface chemistry at nanostructure surfaces as well as the localized surface plasmon biosensing using metallic nanostructures.

1. Introduction

Growing interest has been directed toward metallic nanostructures, such as gold nanospheres and nanorods, because of their interesting optical properties originating from the localized surface plasmons (LSPs).[1−7] LSP is a cooperative oscillation of free electrons in metallic nanostructures and is excited by light at resonant wavelengths. Since the resonant wavelength is sensitive to the surface dielectrics adjacent to the nanostructure surface, it is a good probe for surface binding events.[5−7] This feature is applied to biosensors, which allow us to make a sensitive detection of biological molecules without fluorescence labeling, even in detecting small amounts of samples. In LSP biosensors, the surface of metallic nanostructures is modified with ligand having affinity to analyte. The surface modification is usually carried out by immersion of the metallic nanostructure in a solution in order to form a ligand layer on the nanostructure. In addition, the LSP biosensing is made by exposure of the surface-modified metallic nanostructure to a sample solution for probing the specific binding of analyte to ligand. In both cases, however, it is unknown how the nanostructure surface is covered with ligand or analyte. For instance, the linear relation between the amount of analyte and the signal is questionable if the analyte partially bind to the ligand on the nanospheres. Thus, it is important to answer this question for the understanding of the surface chemistry at nanosphere surfaces and of the optical response of the LSP biosensors.

In this work, we investigate formation process of a self-assembled monolayer (SAM) of hemicyanine-terminated alkanethiolate on surface-immobilized gold nanospheres. We consider it to be a simple model system for the understanding of the surface chemistry and LSP biosensors. We investigated the cap angle, θ_{cap}, of the SAM defined as the polar angle covered with the SAM at the nanosphere surface, as shown in Figure 1a. The cap angle was investigated as a function of immersion time in an ethanolic solution of the hemicyanine-terminated alkane disulfide by use of optical second harmonic generation (SHG) and transmission absorption spectroscopy. SHG is one of the second-order nonlinear optical phenomena, which occurs in a system with no inversion center, under the electric dipole approximation. Hence, it is a powerful probe for surfaces and interfaces, where inversion symmetry is intrinsically absent.[8] It was found that the upper region of the gold nanosphere is initially covered with the hemicyanine SAM, followed by the additional formation of the SAM in the lower region of the nanosphere. We also found that the hemicyanine SAM does not cover the whole surface of the nanosphere even after long exposure to the solution.

2. Experiment

Samples are prepared as the following procedure. A glass substrate was exposed to an ethanolic solution of *N*-(2-aminoethyl)-3-aminopropyltrimethoxysilane (SILA-ACE, S320, Chisso Corp., Japan) with 5% (v/v) of acetic acid at room temperature for 10 min. Then the substrate was rinsed with ethanol and was annealed at 120 °C for silanization. Next, the substrate was immersed in an aqueous solution of gold nanospheres 50 nm in diameter (Tanaka Kikinzoku Kogyo, K. K., Japan) for 2 h. The nanospheres were immobilized on the glass substrate. Finally, the substrates were immersed in an ethanolic solution of the hemicyanine-terminated alkane disulfide[9−11] (Figure 1a) at a 0.01 mM concentration with

*Corresponding author: phone +81-25-924-5596; fax +81-25-924-5596; e-mail kajikawa@ep.titech.ac.jp.

(1) Bohren, C. F.; Huffman, D. R. *Absorption and Scattering of Light by Small Particles*; Wiley: NewYork, 1983.
(2) Abe, S.; Kajikawa, K. *Phys. Rev. B* **2006**, *74*, 035416.
(3) Nie, S.; Emory, S. R. *Science* **1997**, *275*, 1102.
(4) Cai, W.; Chettiar, U. K.; Kildishev, A. V.; Shalaev, V. M. *Nature Photonics* **2007**, *1*, 224.
(5) Haes, A. J.; Van Duyne, R. P. *J. Am. Chem. Soc.* **2002**, *124*, 10596–10604.
(6) Nath, N.; Chilkoti, A. *J. Fluoresc.* **2004**, *14*(4), 377–389.
(7) Mitsui, K.; Handa, Y.; Kajikawa, K. *Appl. Phys. Lett.* **2004**, *85*(18), 4231–4233.
(8) Shen, Y. R. *The Principles of Nonlinear Optics*; Academic Press: New York, 1984; Chapter 25.
(9) Kajikawa, K.; Naraoka, R.; Okawa, H.; Ikezawa, H.; Hashimoto, K. *Mol. Cryst. Liq. Cryst.* **2001**, *370*, 277–283.
(10) Naraoka, R.; Kaise, G.; Kajikawa, K.; Okawa, H.; Ikezawa, Y.; Hashimoto, K. *Chem. Phys. Lett.* **2002**, *362*, 26–30.
(11) Naraoka, R.; Okawa, H.; Hashimoto, K.; Kajikawa, K. *Opt. Commun.* **2005**, *248*, 249–256.

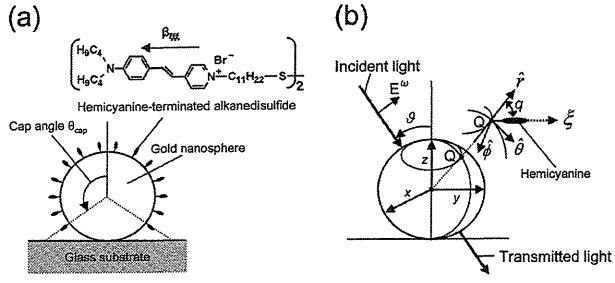

Figure 1. (a) A gold nanosphere capped by hemicyanine SAM with a cap angle θ_{cap}. (b) Geometry for the theoretical calculation.

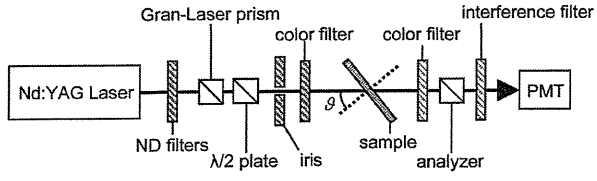

Figure 2. Optical setup used for SHG measurements.

the immersion times ranging from 72 to 72 000 s. The substrates were rinsed with ethanol to remove excess molecules.

The SHG measurements were performed with the optical setup shown in Figure 2. A Nd:YAG laser (LS-2135, LOTIS TII, Ltd., Belarus) operating at 1064 nm was used as a fundamental light source. The repetition frequency was 10 Hz, and the pulse width was 10 ns. The angle of incidence was controlled with a computer. The laser light was incident to the sample with no focusing; the spot size at the sample surface was 5 mm in diameter. A Gran-Laser polarizer and a half-wave plate were used to choose the fundamental polarization. The power density of the fundamental light was reduced to be ~0.1 mJ/mm^2 using neutral density filters. The reflected SHG light was detected with a R-995 photomultiplier tube (PMT, Hamamatsu Photonics K.K., Japan) after removing the fundamental light with color and interference filters. The polarization of the reflected light was selected using a film polarizer. The PMT output was averaged with a SR-250 boxcar integrator (Stanford Research Inc.) for 10 s.

The absorption spectrum was taken with a halogen lamp used as a light source. The light was incident to the sample surface, and the transmitted light was detected with a MCPD-3000 spectrometer (Otsuka Denshi Ltd., Japan). Typical accumulation time was 30 ms.

3. Results and Discussion

3.1. Absorption Measurements. We measured transmission absorption spectra of the samples fabricated with various immersion times in the hemicyanine ethanol solution. Figure 3a plots the relation of the absorption peak wavelength shift with respect to the immersion time. The absorption spectra of the samples with immersion times of 0 and 72 000 s are shown in the inset. In the absorption spectra, a red shift of the LSP peak is observed on binding of a hemicyanine SAM to the gold nanosphere. It seems to be accompanied by slight broadening. The broadening is also observed in another report[12] and in theoretical calculation on the basis of the expressions in ref 13, in which gold nanospheres are covered with a dielectric layer with no optical absorption. This peak shift increases with immersion time, and the red-shifting is almost over at an immersion time of 10 000 s. This means that the hemicyanine SAM formation is complete at the gold nanosphere surface at 10 000 s. The red shift is about 4 nm at saturation.

(12) Okamoto, T.; Yamaguchi, I.; Kobayashi, T. *Opt. Lett.* **2000**, *25*, 372–374.
(13) Neeves, A. E.; Birnboim, M. H. *J. Opt. Soc. Am. B* **1989**, *6*, 787.

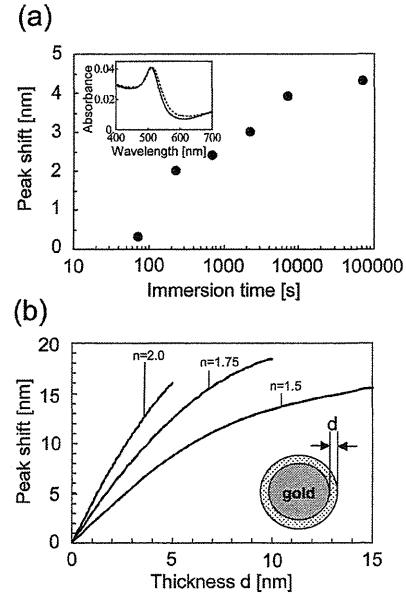

Figure 3. (a) Absorption peak shift as a function of immersion time. Absorption spectra before (solid line) and after (dashed line) deposition of hemicyanine SAMs (immersion time of 72 000 s). (b) Calculated absorption peak wavelength shift as a function of thickness of a covering dielectric film with a refractive index of 1.5, 1.75, and 2.0.

The peak shift is mostly due to a change in the real part of the refractive index of the hemicyanine SAM, while hemicyanine has some optical absorption near the LSP band. This is because the optical density of the hemicyanine monolayer is relatively small (~0.01), according to a spectrum of a hemicyanine Langmuir–Blodgett monolayer.[14] Thus, the contribution of optical absorption is estimated to be less than 0.001, considering the surface number density of the nanosphere of less than 10%. Consequently, we only consider the real component of the refractive index change for the theoretical calculation of the red shift. We calculated absorption spectra of gold nanospheres fully covered with a dielectric film with refractive index of 1.5, 1.75, or 2.0. The refractive index of gold is taken from the literature.[15]

The calculation was made with reference to a previous report.[13] Figure 3b plots the calculated absorption peak wavelength shifts as a function of thickness of the dielectric film. The calculated curve is similar to the experimental results reported previously,[12] suggesting adequacy of this calculation. From this relation, the red shift of 4 nm corresponds to the thickness of the cover layer of 2.0 nm for n = 1.5, 1.3 nm for n = 1.75, and 1.0 nm for n = 2.0. In our previous paper, the thickness of the hemicyanine SAM is evaluated to be 1.2 nm by surface plasmon resonance (SPR) spectroscopy at 633 nm in the attenuated total reflection (ATR) geometry, using the SAM index n = 1.5.[11,16] The thickness of 1.2 nm is somewhat smaller than the evaluated thickness if we use n = 1.5 but is consistent at n = 1.75. The refractive index of the hemicyanine SAM at the LSP resonance wavelength of 530 nm will be larger than that at 633 nm, since the absorption spectrum of the hemicyanine in solution has a peak at 500 nm.[17]

(14) Kajikawa, K.; Shirota, K.; Takezoe, H.; Fukuda, A. *Jpn. J. Appl. Phys.* **1991**, *30*, 362–365.
(15) Johnson, P. B.; Christy, R. W. *Phys. Rev. B* **1972**, *6*, 4370–4379.
(16) Uzawa, R.; Tanaka, D.; Okawa, H.; Hashimoto, K.; Kajikawa, K. *Appl. Phys. Lett.* **2009**, *95*, 021107.
(17) Iiyama, T.; Fukuyo, M.; Naraoka, R.; Okawa, H.; Ikezawa, H.; Hashimoto, K.; Kajikawa, K. *Opt. Commun.* **2007**, *279*, 320–323.

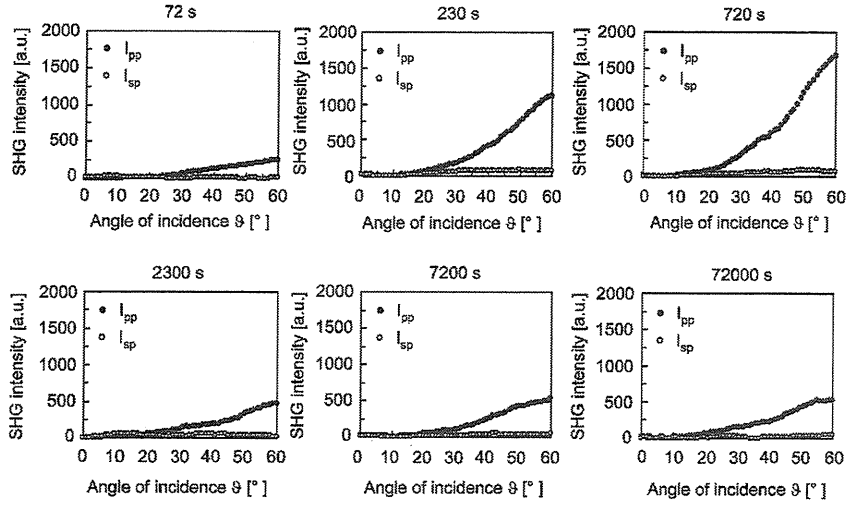

Figure 4. SHG intensity vs ϑ for samples with different immersion times.

Such a large red shift suggests that the gold nanosphere is almost covered with the hemicyanine SAM when the substrate is immersed in the solution for more than 10 000 s. The relation clearly shows that the amount of hemicyanine increases with the immersion time. However, it is not clear, only from the absorption spectra, whether the density of the hemicyanine increases with time or the cap angle increases with time at a constant density.

3.2. SHG Measurement. We performed SHG measurements to clarify how the hemicyanine SAM covers the gold nanospheres. Figure 4 plots p-polarized SHG intensity $I_{pp}(\vartheta)$ excited by p-polarized fundamental light and p-polarized SHG intensity $I_{sp}(\vartheta)$ excited by s-polarized fundamental light as a function of angle of incidence ϑ for samples with different immersion times. SHG is absent at normal incidence, suggesting that SHG from the gold nanosphere is negligibly weak. The SHG intensity monotonically increases with the angle of incidence. $I_{sp}(\vartheta)$'s are much weaker than $I_{pp}(\vartheta)$'s, and some of them are below the noise level ~20.

Figure 5 shows $I_{pp}(60°)$ as a function of the immersion time. The SHG intensity is maximum for the sample with an immersion time of 720 s, although the amount of the red shift increases with the immersion time of more than 720 s as shown in Figure 3a. These results are interpreted as illustrated in Figure 6: the hemicyanine SAM mainly forms in the upper region of the nanosphere, in the early stage, followed by the gradual formation of the hemicyanine SAM in the lower hemisphere region. The SHG light from the upper hemisphere region and that from the lower hemisphere region are canceled, resulting in the decrease in SHG intensity. On the other hand, the LSP red shift increases after the immersion time of 720 s, as shown in Figure 3a, suggesting that the SAM continues to form after 720 s. Even after long exposure to the solution, SHG is not absent. This suggests that the hemicyanine does not cover the whole surface of the nanosphere and SHG is not completely canceled. It is likely that the space under the nanosphere is too narrow to form a hemicyanine SAM.

In order to find the orientation of the hemicyanine SAM, we plotted the SHG intensity ratio, $R(\vartheta) = I_{pp}(\vartheta)/I_{sp}(\vartheta)$, for the samples with immersion times of 230, 720, and 2300 s, in Figure 7. $R(\vartheta)$'s for samples with other than these are excluded because of weak $I_{sp}(\vartheta)$.

3.3. SHG Calculation. If the distance between the nanospheres is small, the electromagnetic interaction between them is not negligible. This interaction causes a new absorption peak at

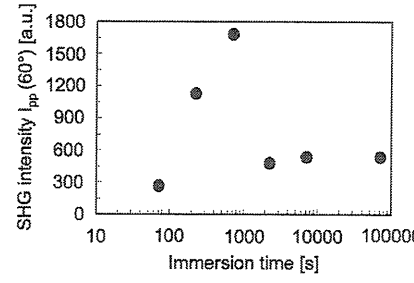

Figure 5. SHG intensity $I_{pp}(60°)$ as a function of immersion time.

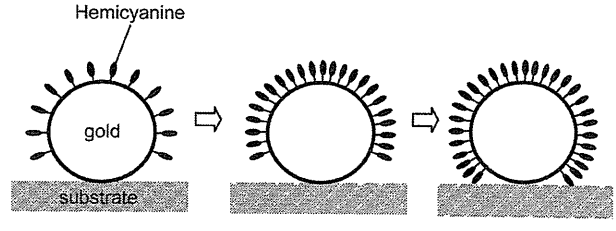

Figure 6. Schematics of the formation process of hemicyanine SAM on a nanosphere surface.

wavelengths of 600−800 nm at normal incidence illumination. Such bands are weak in the absorption spectra as shown in the inset of Figure 3a. Hence, we can regard the nanospheres as of isolation and may consider that the total SHG is the sum of SHG light from a single nanosphere.

The optical geometry for the calculation of the SHG response is illustrated in Figure 1b. The fundamental light at angular frequency ω is incident to the sample surface at an angle of incidence ϑ. The ratio of SHG intensity

$$R(\vartheta) = \frac{I_{pp}(\vartheta)}{I_{sp}(\vartheta)} \quad (1)$$

can be calculated if χ_0/χ_1 and θ_{cap} are provided. Details of the theoretical calculation are given in the Supporting Information.

Since the hemicyanine SAM has $C_{\infty v}$ symmetry with the rotational axis normal to the surface, the susceptibility tensor is composed of two independent components in the molecular coordinates: $\chi_0 = \chi_{rrr}$, $\chi_1 = \chi_{r\theta\theta} = \chi_{r\phi\phi} = \chi_{\theta r\theta} = \chi_{\phi\phi r}$ at point Q.

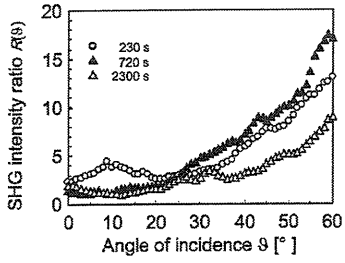

Figure 7. SHG intensity ratio $R(\vartheta)$ for samples with immersion times of 230, 720, and 2300 s.

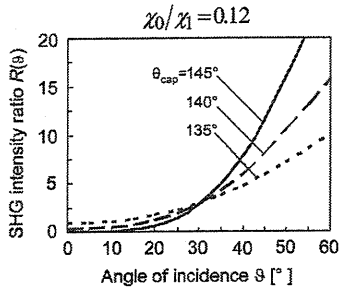

Figure 8. Calculated curves of $R(\vartheta)$ as a function of ϑ and different cap angles at $\chi_0/\chi_1 = 0.12$.

The components χ_0 and χ_1 have the relations

$$\chi_0 = N_{\text{hemi}}\langle\cos^3 q\rangle\beta_{\xi\xi\xi} \tag{2}$$

$$\chi_1 = N_{\text{hemi}}\langle\cos q \sin^2 q\rangle\beta_{\xi\xi\xi} \tag{3}$$

where N_{hemi} is the surface number density of the hemicyanine molecules on the gold nanosphere, q is the tilt angle of the molecule with respect to the surface normal, and $\beta_{\xi\xi\xi}$ is the molecular polarizability in the molecular coordinates, as shown in Figure 1b. Hemicyanine is assumed to have a dominant molecular polarizability component along the molecular long axis ξ because of the rodlike structure. The bracket is the average over the molecules.

Figure 8 shows a theoretical $R(\vartheta)$ curves calculated at $\chi_0/\chi_1 = 0.12$ for $\theta_{\text{cap}} = 135°$, 140°, and 145°. The χ ratio $\chi_0/\chi_1 = 0.12$ is experimentally obtained, as described below. Since the profiles with a cap angle θ_{cap} are identical to those with a cap angle $180° - \theta_{\text{cap}}$, they are impossible to be distinguished only from the SHG measurements. However, we can choose the $\theta_{\text{cap}} > 90°$ because of the LSP shift in Figure 3a. Calculated $R(\vartheta)$ curves for other parameters are given in Figure S1 of the Supporting Information. The calculation of the $R(\vartheta)$ profile is so intricate that it is considerably time-consuming. Hence, it is impossible to make the fitting of the experimental $R(\vartheta)$ curve to the theoretical one within realistic time, although it is one of the best way to obtain the parameters of χ_0/χ_1 and θ_{cap}. Instead, we evaluated the parameters from $R(45°)$ and $R(\vartheta\rightarrow 0°)$ (extrapolation toward 0°), denoted by $R(0°)$ below. Figure 9a plots the relation between χ_0/χ_1 and θ_{cap} at $R(0°) = 2.3$ and $R(45°) = 7.8$. The $R(0°)$ and $R(45°)$ values are taken from experimental results of the sample with an immersion time of 230 s. Figures 9b and 9c also plot the relations at ($R(0°) = 1.5$, $R(45°) = 8.6$) and ($R(0°) = 1.9$, $R(45°) = 4.2$), respectively. They are taken from the samples with immersion times of 720 and 2300 s. The intersection of both experimental curves $R(0°)$ and $R(45°)$ gives the parameters of χ_0/χ_1 and θ_{cap}. Thereby, we evaluated the χ_0/χ_1 and θ_{cap} parameters in Table 1. Although there are two possible θ_{cap} values, they are too close to be separated, considering the

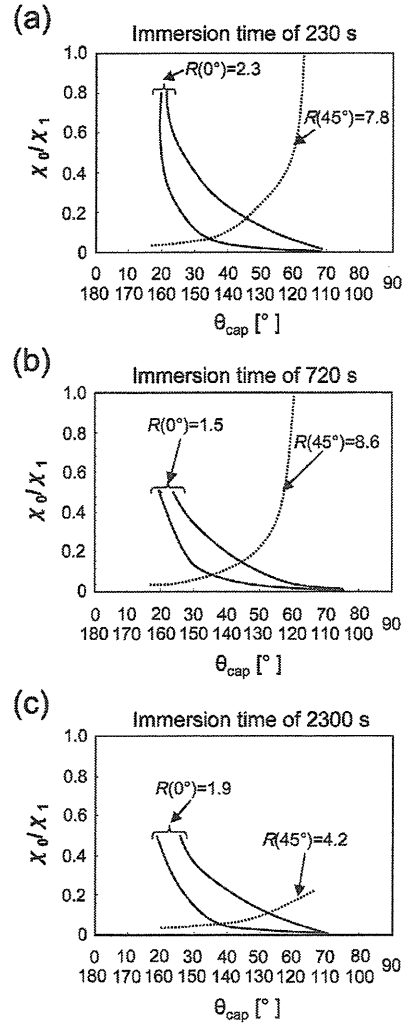

Figure 9. Plots of $R(0°)$ and $R(45°)$ as a function of χ_0/χ_1 and θ_{cap}. (a) $R(0°) = 2.3$ and $R(45°) = 7.8$, (b) $R(0°) = 1.5$ and $R(45°) = 8.6$, and (c) $R(0°) = 1.9$ and $R(4.2°) = 4.2$. They are taken from the results of the samples with immersion times of 230, 720, and 2300 s.

Table 1. Experimental Values of θ_{cap} [deg] and χ_0/χ_1 for the Samples with Immersion Times of 230, 720, and 2300 s

immersion time (s)	θ_{cap} [deg]	χ_0/χ_1
230	135	0.17
	146	0.10
720	136	0.15
	145	0.09
2300	128	0.13
	143	0.07

experimental errors. Thus, we conclude that the average cap angle is $\theta_{\text{cap}} = 139 \pm 11°$ and $\chi_0/\chi_1 = 0.12 \pm 0.05$ for the samples having great SHG activity.

The susceptibility ratio $\chi_0/\chi_1 = 0.12$ gives the average tilt angle of $\langle q\rangle = 76°$ since eqs 2 and 3 give the relation

$$\langle q\rangle \simeq \tan^{-1}\sqrt{\frac{2\chi_1}{\chi_0}} \tag{4}$$

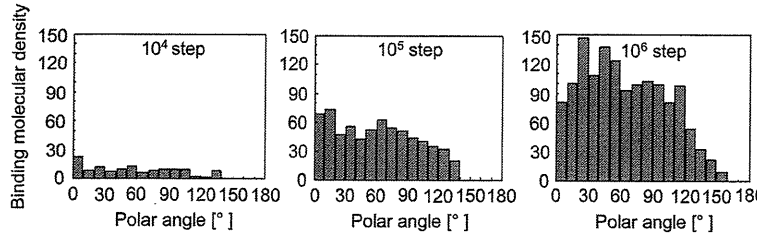

Figure 10. Histograms of binding molecular density on the surface of a nanosphere, obtained by the Monte Carlo simulation after 10^4, 10^5, and 10^6 steps.

Our SHG measurements for the hemicyanine SAM formed on a flat gold substrate give the SHG intensity ratio $R(\vartheta) = I_{pp}(\vartheta)/I_{sp}(\vartheta) = 270$ and $\chi_0/\chi_1 = 0.6$, with which the average tilt angle is calculated to be $\langle q \rangle = 61°$. The difference in the average tilt angle is only 15°. Namely, the hemicyanine molecules on gold nanospheres have orientation similar to that of hemicyanine on a flat gold substrate.

3.4. Monte Carlo Simulation. We performed a Monte Carlo simulation on the binding of the hemicyanine-terminated alkane disulfide to the gold nanosphere surface to support the schematic picture depicted in Figure 6. A gold nanosphere with a radius of 25 is located in a cubic space with a dimension of 200 × 200 × 200, where 10^3 molecules are randomly placed. This density is equal to 0.2 mM. If the molecule is placed inside the nanosphere, they are removed. Each molecule moves by a distance of 1 in a random direction, at each step. When a molecule bumps against the nanosphere surface, it is assumed to be immobilized at the surface. When a molecule bumps against the boundary or the substrate surface, the molecule is assumed to be reflected elastically. For simplicity, the calculation was made with neglecting the volume of molecules.

Figure 10 shows histograms of the binding molecular density with respect to the polar angle after the calculation of 10^4–10^6 steps. It is clear that molecules binding at polar angles of more than 140° is few. This is because the space below the nanosphere is narrow and the adsorption is diffusion-controlled at this concentration, where average intermolecular distance is about 20 nm (cubic lattice model). This simulated result is qualitatively in agreement with the experimental observation.

4. Conclusion

We have investigated formation of a hemicyanine-terminated alkanethiolate SAM on a gold nanosphere surface by use of absorption spectroscopy, optical SHG measurements, and Monte Carlo simulation. It was found that the hemicyanine SAMs mainly form in the upper hemisphere region (the cap angle is ~140°) in the early stage, followed by formation of the SAM in the lower region of the nanosphere. Namely, the SAM does not homogeneously form over the nanosphere surface, and the hemicyanine SAM does not cover the whole surface of the nanosphere even after long exposure to the solution. In addition, it was found that the orientation of the hemicyanine molecules on gold nanospheres is similar to that of hemicyanine on a flat gold substrate. The Monte Carlo simulation suggests that the binding of the hemicyanine-terminated alkane disulfide to the surface is a diffusion-controlled reaction in the narrow space under the nanosphere. Both experimental and simulation results are qualitatively in agreement. We also propose an analytical expression of SHG from a molecular monolayer on a nanosphere surface. These results are important to understand the surface chemistry at nanostructure surfaces as well as the localized surface plasmon biosensing using metallic nanostructures. Particularly, the theoretical expression of the LSP response for a partial core–shell model is needed for the analysis of LSP biosensing using gold nanospheres. This work is in progress and will be reported elsewhere.

Supporting Information Available: Theoretical description of SHG intensity from the hemicyanine SAM on a surface-immobilized nanosphere and calculated $R(\vartheta)$ (Figure 1S) curves. This material is available free of charge via the Internet at http://pubs.acs.org.

Bioorganic & Medicinal Chemistry 18 (2010) 2402–2411

Contents lists available at ScienceDirect

Bioorganic & Medicinal Chemistry

journal homepage: www.elsevier.com/locate/bmc

Structural development studies of anti-hepatitis C virus agents with a phenanthridinone skeleton

Masahiko Nakamura [a], Atsushi Aoyama [a], Mohammed T. A. Salim [b], Mika Okamoto [b], Masanori Baba [b,*], Hiroyuki Miyachi [c], Yuichi Hashimoto [a], Hiroshi Aoyama [a,*]

[a] Institute of Molecular & Cellular Biosciences, The University of Tokyo, 1-1-1 Yayoi, Bunkyo-ku, Tokyo 113-0032, Japan
[b] Division of Antiviral Chemotherapy, Center for Chronic Viral Diseases, Graduate School of Medical and Dental Sciences, Kagoshima University, 8-35-1 Sakuragaoka, Kagoshima 890-8544, Japan
[c] Division of Pharmaceutical Sciences, Okayama University Graduate School of Medicine, Dentistry and Pharmaceutical Sciences, 1-1-1 Tsushima-Naka, Kita-ku, Okayama 700-8530, Japan

ARTICLE INFO

Article history:
Received 10 February 2010
Revised 24 February 2010
Accepted 25 February 2010
Available online 2 March 2010

Keywords:
Anti-HCV agents
Phenanthridinone
Thalidomide
Am80
Am580

ABSTRACT

A phenanthridinone skeleton was derived from our previous researches on thalidomide and retinoids as a multi-template for generation of anti-viral lead compounds. Structural development studies focusing on anti-hepatitis C virus activity afforded 5-butyl-2-(1,1,1,3,3,3-hexafluoro-2-hydroxypropan-2-yl)phenanthridin-6(5*H*)-one (**10**) and 5-butylbenzo[*b*]phenanthridin-6(5*H*)-one (**39**), which showed EC_{50} values of approximately 3.7 and 3.2 μM, respectively.

1. Introduction

The efficient identification of small-molecular scaffolds for the development of biologically active compounds is very important in chemical genetics and medicinal chemistry. As one approach, we have been utilizing the multi-template hypothesis,[1–5] based on the idea that the number of protein fold structure types that comprise all the domains occurring in natural proteins is quite limited, in spite of the huge number of natural proteins.[6–8] A given fold structure might be characteristic of many natural proteins, and therefore, ignoring physical/chemical interactions, one might expect that a template/scaffold structure which is spatially complementary to one fold structure might serve as a multi-template for structural development of ligands that would interact specifically with many different natural proteins. As candidate multi-template structures, we have focused particularly on thalidomide (**1**) and retinoids, including synthetic retinoids Am80 (**2**) and Am580 (**3**) (Fig. 1).[1,9–13] All of these compounds **1–3** elicit a wide range of biological activities, and thalidomide (**1**) is well-established to be multi-target drug.[1,9–13] In fact, we recently applied thalidomide (**1**) and/or Am80 (**2**)/Am580 (**3**) as multi-templates to develop anti-viral agents and/or anti-proliferative agents for virus-infected cells, that is, anti-bovine viral diarrhea virus (anti-BVDV) agents, including SK3M4M5M (**4**) derived from thalidomide (**1**)[14,15] and adult T-cell leukemia (ATL) cell-selective proliferation inhibitors, including TMN($COCH_3$) (**5**) and TMN(OH)($COCH_3$) (**6**) derived from Am80 (**2**)/Am580 (**3**) (Fig. 1).[4] We next aimed to develop anti-hepatitis C virus (HCV) agents.

HCV infection is thought to be a major cause of human hepatitis,[16,17] and it is estimated that at least 170 million people worldwide are chronically infected with this virus.[18] Most infections become persistent and about 60% of cases progress to chronic liver disease, which in turn can lead to development of cirrhosis, hepatocellular carcinoma, and liver failure.[19,20] Currently, no vaccine is available against HCV infection, and the standard treatment for chronic hepatitis C consists of pegylated interferon (IFN)-α in combination with the nucleoside analog ribavirin (1-β-D-ribofuranosyl-1,2,4-triaxole-3-carboxamide). However, the virus cannot be eliminated from approximately half of infected patients treated with these agents.[21] In addition, the side effects of these agents are sometimes serious and unacceptable to patients. Therefore, alternative agents for the treatment and prevention of HCV infection are urgently needed.

As mentioned above, we have been succeeded in the development of potent anti-BVDV agents, including SK3M4M5M (**4**), which

* Corresponding authors. Tel.: +81 3 5841 7848; fax: +81 5841 8495 (H.A.); tel.: +81 99 275 5930; fax: +81 99 275 5932 (M.B.).
E-mail addresses: m-baba@vanilla.ocn.ne.jp (M. Baba), aoyama@iam.u-tokyo.ac.jp (H. Aoyama).

0968-0896/$ - see front matter © 2010 Elsevier Ltd. All rights reserved.
doi:10.1016/j.bmc.2010.02.057

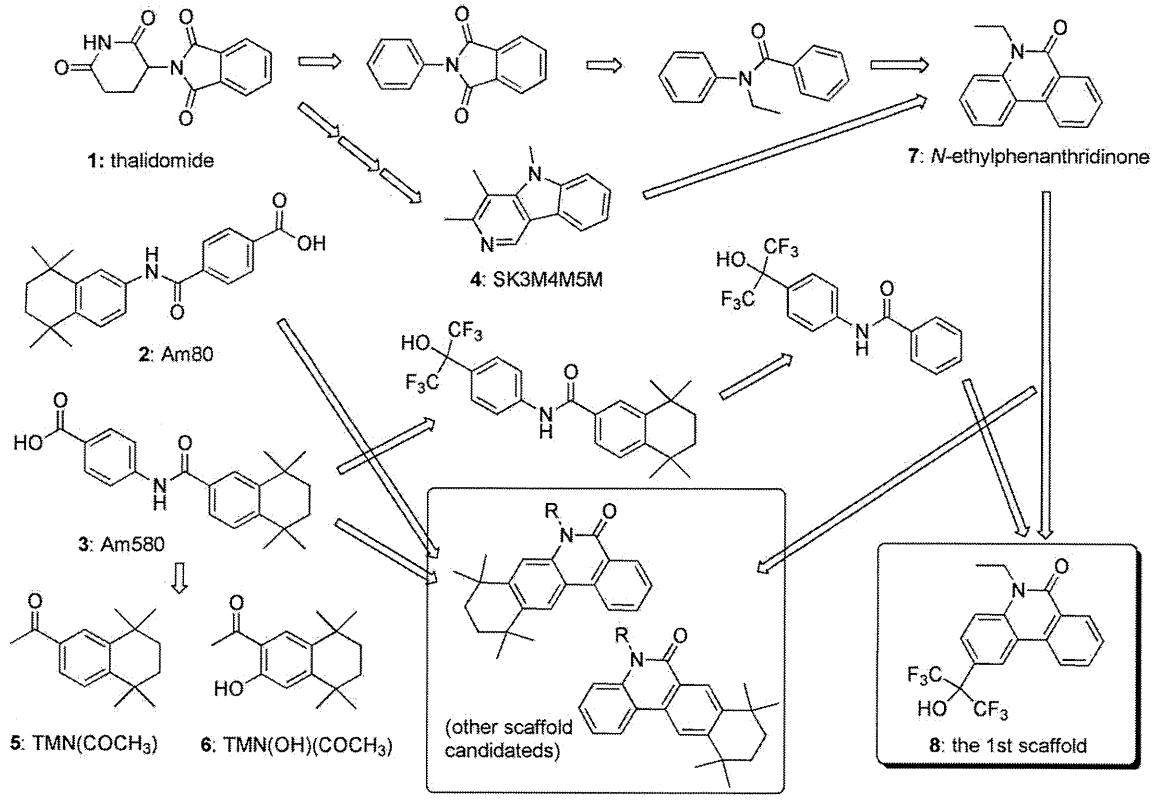

Figure 1. Armchair structural development of thalidomide (**1**) and retinoids (**2**, **3**) to the first scaffold **8**.

have an EC_{50} value of 3.5 nM.[15] Although BVDV belongs to the *Flaviviridae* family, as HCV does,[22] and is thought to be a surrogate model for HCV,[23–25] SK3M4M5M (**4**) showed only a very weak activity against HCV. Therefore, we tried to develop another scaffold for the development of anti-HCV agents, as shown in Figure 1.

2. Results and discussion

2.1. Armchair structural development leading to phenanthridinone derivatives

First, we applied armchair structural development to phenylphthalimide, which was itself developed from thalidomide (**1**). The phenylphthalimide skeleton is a superior multi-template, and we have developed various biologically active phenylphthalimide derivatives, including tumor necrosis factor-α production regulators, tubulin polymerization inhibitors, dipeptidylpeptidase type IV inhibitors, liver X receptor antagonists, α-glucosidase inhibitors, and so on.[1,9–12] The armchair ring opening of phenylphthalimide gave *N*-ethylbenzanilide, whose recyclization should afford *N*-ethylphenanthridinone (**7**) (Fig. 1). On the other hand, synthetic retinoids Am80 (**2**) and Am580 (**3**) both possess a benzoic acid moiety. Because our previous studies on anti-BVDV agents suggested that carboxyl acid derivatives are not suitable as lead structures, we considered that a bioisosteric functional group, the 1,1,1,3,3,3-hexafluoropropan-2-ol-substituted phenyl moiety, might be introduced into *N*-ethylphenanthridinone (**7**) to give the first scaffold structure, 5-ethyl-2-(1,1,1,3,3,3-hexafluoro-2-hydroxypropan-2-yl) phenanthridin-6(5*H*)-one (**8**) (Fig. 1). In addition, both Am80 (**2**) and Am580 (**3**) possess a teterahydrotetramethylnaphthalene moiety, which has been established to be a useful core structure to develop ATL cell-selective proliferation inhibitors, including $TMN(COCH_3)$ (**5**) and $TMN(OH)(COCH_3)$ (**6**).[4] We therefore considered that docking of teterahydrotetramethylnaphthalene moiety and *N*-ethylphenanthridinone (**7**) would afford other scaffold candidate structures, as shown in Figure 1.

Compound **8** was prepared as shown in Scheme 1.[26,27] Briefly, *N*-ethylaniline was treated with hexafluoroacetone to give the 1,1,1,3,3,3-hexafluoro-2-hydroxypropyl derivative, which was coupled with 2-iodobenzoyl chloride. The resulting anilide was cyclized to give compound **8**. The anti-HCV activity of compound **8** was determined in the established HCV RNA replicon cells.[28] Briefly, NNC #2 cells carrying full-genomic HCV RNA replicons were cultured in the presence of various concentrations of the test compounds for 3 days. The cells were examined for HCV RNA and glyceraldehyde-3-phosphate dehydrogenase (GAPDH) RNA levels by real-time reverse transcription (RT)-PCR. The anti-HCV activity and cytotoxicity of test compounds were expressed as 50% effective concentration (EC_{50}) and 50% cytotoxic concentration (CC_{50}), defined in terms of decrease of HCV RNA and GAPDH RNA levels to 50% of the respective control levels. As shown in Figure 2, compound **8** showed apparent anti-HCV activity (EC_{50} and CC_{50}: 14.1 and >40 μM, respectively), suggesting that compound **8** could be a lead compound for structural development of anti-HCV agents.

2.2. Effects of N-substituents

Since compound **8** showed anti-HCV activity, we examined the effects of *N*-substituents. Several N-alkylated derivatives of **8** (**9**–**14**) were prepared as shown in Scheme 2, and their anti-HCV activity was measured as described above (Figs. 2 and 3).

As shown in Figures 2 and 3, introduction of three fluorine atoms at the terminal methyl group (**9**) did not improve the activity. However, introduction of a longer-chain alkyl group, *n*-butyl (**10**), *n*-hexyl (**11**), or *n*-nonyl (**12**), resulted in enhancement of anti-HCV activity, though at the same time, the cytotoxicity was increased. The anti-HCV activity of these compounds decreased

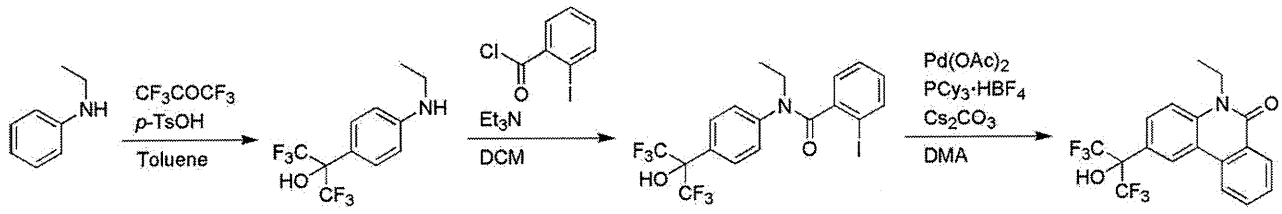

Scheme 1.

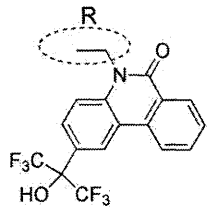

R	EC_{50} (μM)	CC_{50} (μM)
8: CH_3CH_2-	14.1	>40
9: CF_3CH_2-	24.8	30.3
10: $CH_3(CH_2)_3$-	3.7	12.5
11: $CH_3(CH_2)_5$-	4.8	12.2
12: $CH_3(CH_2)_8$-	8.3	10.2
13: $PhCH_2$-	7.7	18.2
14: c-$C_6H_{11}CH_2$-	6.7	14.4

Figure 2. Effects of N-substituents on anti-HCV activity. EC_{50}: 50% effective concentration, based on the decrease of the amount of HCV RNA. CC_{50}: 50% cytotoxic concentration, based on the decrease of the amount of GAPDH RNA.

in the order of: **10** > **11** > **12**. On the other hand, their cytotoxicity tended to decrease in the reverse order, though the differences were small. The benzyl analog (**13**) and the cyclohexylmethyl analog (**14**) showed moderate anti-HCV activity (EC_{50}: 7.7 and 6.7 μM, respectively) with weaker cytotoxicity (CC_{50}: 18.2 and 14.4 μM, respectively). Cytotoxicity was not affected by the length of the introduced alkyl group (CC_{50}: 10.2–12.5 μM). Among this series, compound **10** showed the most potent anti-HCV activity (EC_{50}: 3.7 μM). Therefore, we selected the *N*-butylphenanthridinone skeleton (corresponding to compound **10**) as a scaffold structure for further structural development studies.

2.3. Regioisomers of methyl-substituted *N*-butylphenanthridinone

Based on our previous structure–activity relationship studies of anti-BVDV γ-carboline analogs, which indicated that regio-selective methyl-substitution dramatically influenced the anti-viral activity,[14,15] the effect of methyl-substitution was investigated. For this purpose, we synthesized all the regioisomers of methyl-

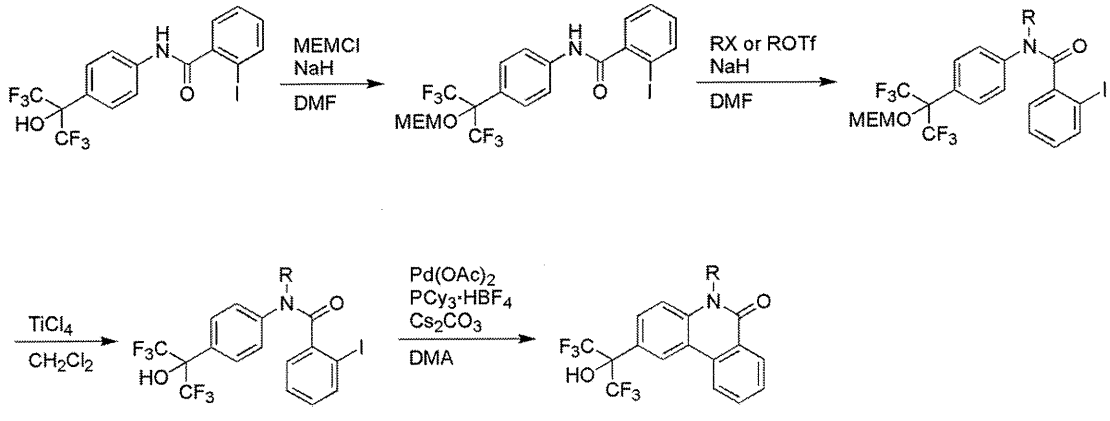

Scheme 2.

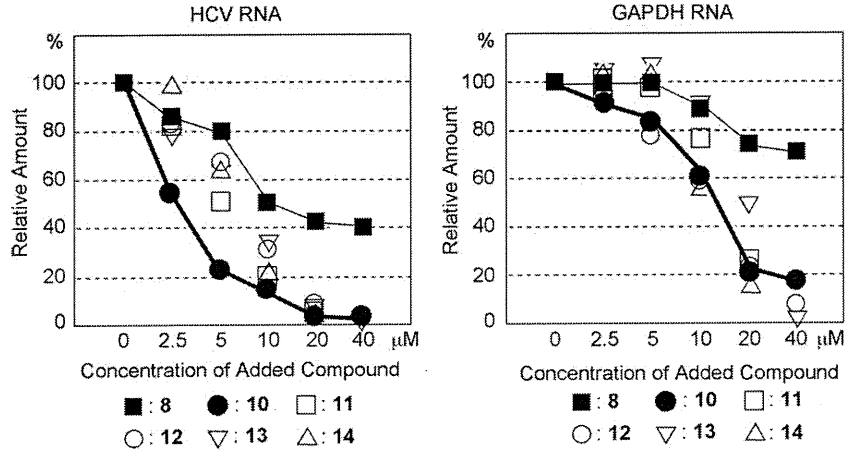

Figure 3. Dose-dependency curves of anti-HCV and cytotoxic activity elicited by compounds **8** and **10–14**.

substituted *N*-butylphenanthridinone (Fig. 4) by the method shown in Scheme 3.

As shown in Figure 4, *N*-butylphenanthridinone itself (an extracted structure from compound **10**) was completely inactive. However, methyl-substitution at position 2, that is, the position at which the 1,1,1,3,3,3-hexafluoropropan-2-ol group was attached in compound **10**, resulted in the appearance of anti-HCV activity (EC_{50}: 42.0 μM). All the other regioisomers, except the 8-methyl analog (**21**), that is, compounds **16**, **18–20**, **22**, and **23**, were inactive, and the anti-HCV activity elicited by **21** was very weak. Therefore, position 2 seems to be the best position at which to introduce a substituent.

2.4. Effect of 2-subsituents on anti-HCV activity

The results described above prompted us to examine the effect of 2-substitutents, and we prepared various derivatives (**24–33**) as shown in Figure 5. Although some derivatives, including compounds **28–33**, showed improved anti-HCV activity compared to the 2-methyl analog **17**, their activity was weaker than that of **10**. As already mentioned, the unsubstituted analog **15** was inactive. Its fluoro analog **24** was also inactive, suggesting that a mono-atomic substituent is inappropriate to improve the activity. Though the 2-methyl analog **17** showed some activity (EC_{50}: 35.8 μM), its trifluoromethyl analog **26** was inactive. On the contrary, its hydroxyl analog **25** showed activity comparable to that of the 2-methyl analog **17**. The 2-ethyl analog **27** also showed activity comparable to that of **17**/**25**.

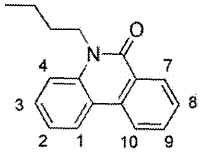

%-Inhibition of HCV gene and host cell gene (GAPDH) expression at 10 μM

	HCV	GAPDH
15: none	inactive	inactive
16: 1-CH_3	inactive	85.2
17: 2-CH_3	42.0	98.5
18: 3-CH_3	inactive	70.7
19: 4-CH_3	inactive	inactive
20: 7-CH_3	inactive	inactive
21: 8-CH_3	87.0	88.8
22: 9-CH_3	inactive	inactive
23: 10-CH_3	inactive	94.9

Figure 4. Anti-HCV activity of methyl-substituted regioisomers of *N*-butylphenanthridinone, **16–23**.

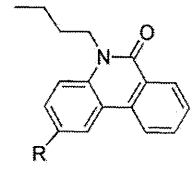

R	EC_{50} (μM)	CC_{50} (μM)
10: $(CF_3)_2(OH)C$-	3.7	12.5
15: H	>58.3	58.3
17: CH_3	35.8	38.4
24: F	>50	>50
25: OH	37.9	43.7
26: CF_3	>50	>50
27: CH_3CH_2	34.7	40.5
28: $(CH_3)_2CH$-	16.2	29.7
29: CH_2OH	21.5	>50
30: $CH_3CH(OH)$-	21.8	51.4
31: $(CH_3)_3CH$	10.6	24.9
32: CH_3CO-	18.7	27.3
33: $Ph(CH_2)_2$-	21.0	24.1

Figure 5. Anti-HCV activity of 2-substituted *N*-butylphenanthridinone, **15**, **17** and **24–33**.

Compounds **28–33** showed moderate anti-HCV activity (EC_{50}: 10.6–21.8 μM). Among the 2-alkylated derivatives, the activity decreased in the order of *t*-butyl (**31**) > *i*-propyl (**28**) > ethyl (**27**) > methyl (**17**), suggesting that the hydrophobicity of the 2-substituent contributes to the activity, at least in part. On the other hand, introduction of a hydroxyl group into the ethyl (**30**) or methyl (**29**) group of **27** and **17**, respectively, seemed to slightly enhance the activity, that is, **27** (EC_{50}: 34.7 μM) versus **30** (EC_{50}: 21.8 μM) and **17** (EC_{50}: 35.8 μM) versus **29** (EC_{50}: 21.5 μM). The 2-acetyl derivative **32** showed slightly more potent activity than **30**.

2.5. Tetrahydrotetramethylnaphthalene-related analogs and benzophenanthridinone analogs

Although the structure–activity relationships of 2-substituted *N*-butylphenanthridinone were clearly interpretable, hydrophobicity around the 2-position also seemed to contribute to the activity. This and the armchair structural development shown in Figure 1 prompted us to prepare compounds **34–38** (Fig. 6). We also prepared benzophenanthridinone derivatives **39–44** (Fig. 7). Among the tetrahydrotetramethylnaphthalene-related analogs **34–38**, only the *N*-butyl and *N*-benzyl derivatives (**35** and **36**, respectively) were moderately active, as shown in Figure 6. The regioisomer of **35**, that is, compound **38**, was inactive.

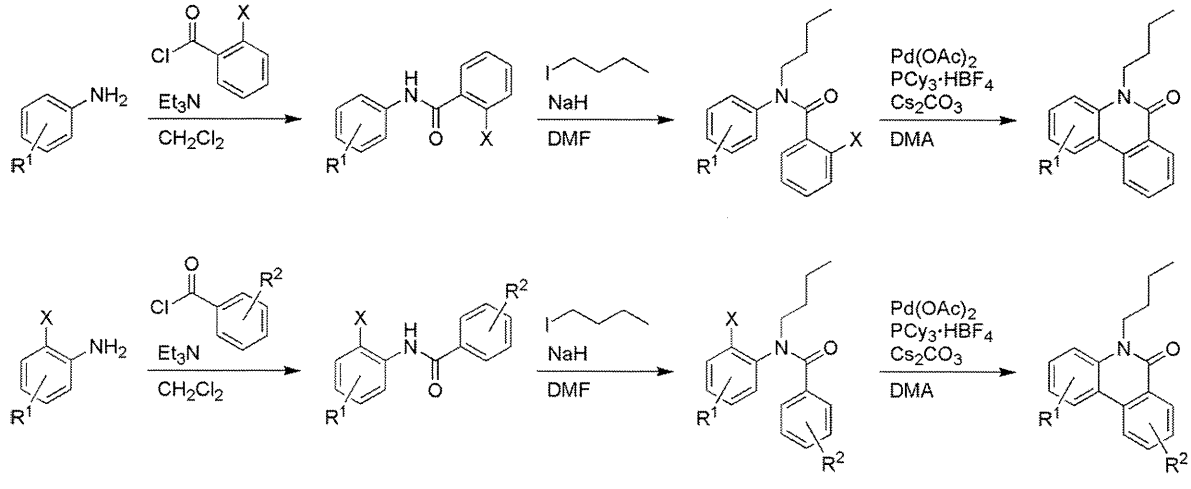

Scheme 3.

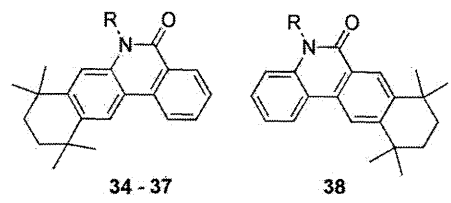

R	EC_{50} (μM)	CC_{50} (μM)
34: H	inactive	inactive
35: $CH_3(CH_2)_3$-	18.7	27.3
36: $PhCH_2$-	21.2	31.8
37: c-$C_6H_{11}CH_2$-	inactive	inactive
38: $CH_3(CH_2)_3$-	inactive	inactive

Figure 6. Anti-HCV activity of tetrahydrotetramethylnaphthalene-related analogs, **34–38**.

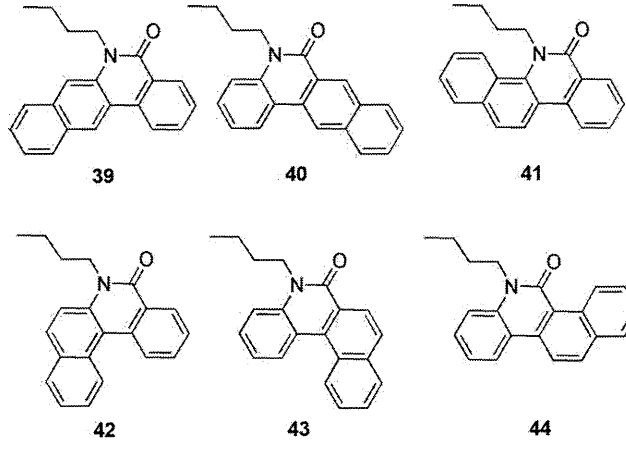

	EC_{50} (μM)	CC_{50} (μM)
35	18.7	27.3
39	3.2	6.3
40	11.0	>40
41	19.5	24.3
42	29.1	44.5
43	>31.4	31.4
44	29.9	>40

Figure 7. Anti-HCV activity of benzophenathridinone derivatives, **39–44**.

Benzophenanthridinone derivatives **39–44** were prepared as shown in Scheme 4. All the benzophenanthridinone derivatives, except **43**, showed potent or moderate anti-HCV activity. The activity decreased in the order of: benzo[*b*] (**39**) > benzo[*j*] (**40**) > benzo[*c*] (**41**) > benzo[*a*] (**42**) > benzo[*i*] (**44**) >> benzo[*k*] (**43**) as shown in Figures 7 and 8. Although compound **39** showed the most

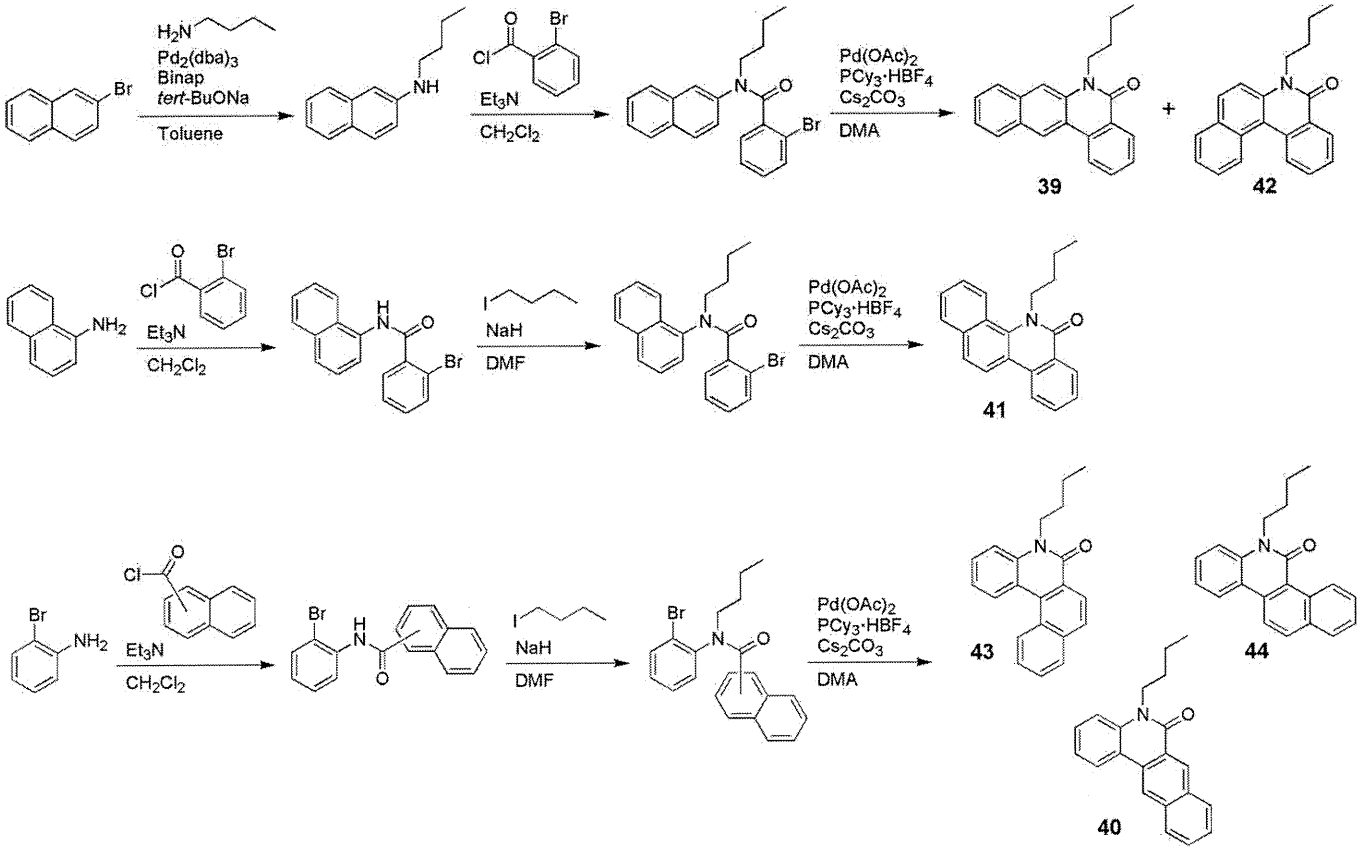

Scheme 4.

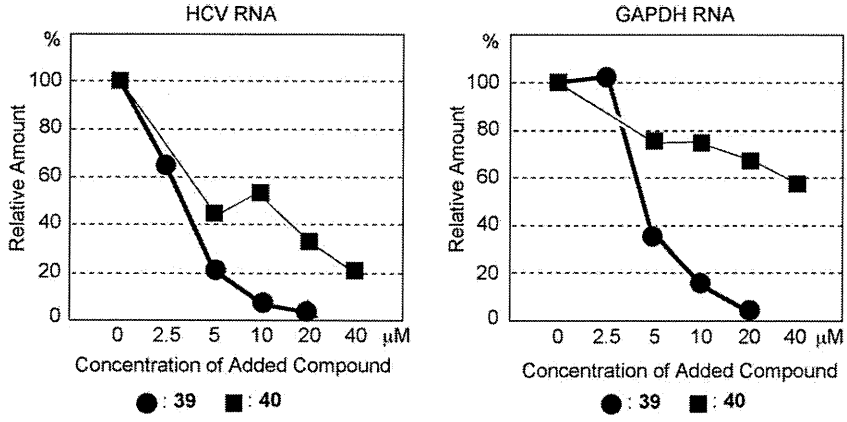

Figure 8. Dose-dependency curves of anti-HCV and cytotoxic activity elicited by compounds **39** and **40**.

potent anti-HCV activity (EC_{50}: 3.2 μM) among the compounds in this paper, its selectivity index (SI = CC_{50}/EC_{50}) was low (SI: 1.97). In terms of SI, compound **40** (EC_{50}: 11.0 μM) seems to be the best (SI: >3.64).

3. Conclusion

Based on a phenanthridinone skeleton derived by armchair structural development of thalidomide and retinoids, we developed candidate anti-HCV agents, **10** (EC_{50}: 3.7 μM,), **39** (EC_{50}: 3.2 μM,), and **40** (EC_{50}: 11 μM, CC_{50}: >40 μM). Further structural development may yield highly potent and selective drug candidates.

4. Experimental

4.1. General comments

Melting points were determined by using a Yanagimoto hot-stage melting point apparatus and are uncorrected. ^{1}H NMR spectra were recorded on a JEOL JNM-GX500 (500 MHz) spectrometer. Chemical shifts are expressed in δ (ppm) values with tetramethylsilane (TMS) as an internal reference. The following abbreviations are used: s = singlet, d = doublet, t = triplet, m = multiplet, dd = double doublet, dt = double triplet, br = broad. Mass spectra (MS) and high-resolution mass spectra (HRMS) were recorded on a JEOL JMS-DX303 spectrometer. Elemental analysis was performed with a Yanagimoto MT-6 elemental analyser.

4.2. 5-Ethyl-2-(1,1,1,3,3,3-hexafluoro-2-hydroxypropan-2-yl)-phenanthridin-6(5*H*)-one (8)

To a solution of 5 mmol of *N*-ethylaniline and 25 mL of toluene were added hexafluoroacetone trihydrate (1.2 equiv) and *p*-TsOH (0.1 equiv). The mixture was stirred for 22 h at 120 °C and the solvent was evaporated in vacuo. The residue was purified by silica gel column chromatography (eluent; *n*-hexane/ethyl acetate) to afford 2-(4-ethylaminophenyl)-1,1,1,3,3,3-hexafluoropropan-2-ol. The obtained compound was dissolved in dichloromethane (0.1 mmol/mL), and then triethylamine (1:40 v/v) and 2-iodobenzoyl chloride (1.2 equiv) were added. The mixture was stirred for 15 h at room temperature and the solvent was evaporated in vacuo. The residue was purified by silica gel column chromatography (eluent; *n*-hexane/ethyl acetate) to afford benzanilide derivatives. To a solution of the obtained benzanilide derivative, cesium carbonate (2 equiv) and *N*,*N*-dimethylacetamide were added palladium (II) acetate (10 mol %) and tricyclohexylphosphine tetrafluoroborate (0.15 equiv), and the mixture was heated to 130 °C. The catalyst was filtered off and washed several times with ethyl acetate. The combined organic layers were washed with water and brine successively, dried over anhydrous magnesium sulfate, and concentrated. The residue was purified by silica gel column chromatography (eluent; *n*-hexane/ethyl acetate) to afford 5-ethyl-2-(1,1,1,3,3,3-hexafluoro-2-hydroxypropan-2-yl)phenanthridin-6(5*H*)-one (**8**) as a white solid. Mp 208.0–209.0 °C. ^{1}H NMR (500 MHz, $CDCl_3$) δ 8.68 (d, J = 1.5 Hz, 1H), 8.56 (dd, J = 7.9, 1.5 Hz, 1H), 8.31 (d, J = 7.9 Hz, 1H), 7.85 (d, J = 9.4 Hz, 1H), 7.80 (td, J = 7.9, 1.3 Hz, 1H), 7.63 (t, J = 7.7 Hz, 1H), 7.50 (d, J = 9.0 Hz, 1H), 4.48 (q, J = 7.3 Hz, 2H), 3.71 (s, 1H), 1.44 (t, J = 7.3 Hz, 3H). HRMS (FAB) calcd for $C_{18}H_{14}F_6NO_2$ 390.0929; found: 390.0918 $(M+H)^+$.

4.3. 2-(1,1,1,3,3,3-Hexafluoro-2-hydroxypropan-2-yl)-5-(2,2,2-trifluoroethyl)phenanthridin-6(5*H*)-one (9)

The title compound was prepared by a method similar to that described for the synthesis of **8**, using aniline as a starting material, with slight modifications. 2-(4-Aminophenyl)-1,1,1,3,3,3-hexafluoropropan-2-ol (prepared from aniline and 1,1,1,3,3,3-hexafluoroacetone)[29] was coupled with 2-iodobenzoyl chloride, followed by protection of the hydroxyl group with 2-methoxylethoxymethyl chloride. It was then N-alkylated by the use of 2,2,2-trifluoroethyl triflate. The 2-methoxyethoxymethyl group of the obtained benzanilide derivative was removed by treatment with titanium tetrachloride, and the deprotected benzanilide derivative was cyclized by the method used for the synthesis of **8**. White solid. Mp 76.1–77.8 °C. ^{1}H NMR (500 MHz, $CDCl_3$) δ 8.70 (d, J = 1.1 Hz, 1H), 8.56 (dd, J = 8.1, 1.1 Hz, 1H), 8.33 (d, J = 8.1 Hz, 1H), 7.87 (dd, J = 7.7, 1.1 Hz, 1H), 7.85 (dd, J = 7.7, 1.1 Hz, 1H), 7.66 (td, J = 8.1 Hz, 1H), 7.51 (d, J = 9.0 Hz, 1H), 5.13 (s, 2H), 3.78 (s, 1H). HRMS (FAB) calcd for $C_{18}H_{10}F_9NO_2$ 444.0646; found: 444.0653 $(M+H)^+$.

4.4. 5-Butyl-2-(1,1,1,3,3,3-hexafluoro-2-hydroxypropan-2-yl)-phenanthridin-6(5*H*)-one (10)

The title compound was prepared by a method similar to that described for the synthesis of **9** using 1-iodobutane instead of 2,2,2-trifluoroethyl triflate. White solid. Mp 166.0–166.6 °C. ^{1}H NMR (500 MHz, $CDCl_3$) δ 8.67 (s, 1H), 8.55 (d, J = 7.9 Hz, 1H), 8.30 (d, J = 7.9 Hz, 1H), 7.84 (d, J = 7.9 Hz, 1H), 7.79 (dd, J = 7.9, 7.3 Hz, 1H), 7.62 (dd, J = 7.9, 7.3 Hz, 1H), 7.47 (d, J = 7.9 Hz, 1H), 4.39 (t, J = 7.9 Hz, 2H), 3.81 (s, 1H), 1.83–1.76 (m, 2H), 1.56–1.50 (m, 2H),

1.03 (t, J = 7.3 Hz, 3H). HRMS (FAB) calcd for $C_{20}H_{18}F_6NO_2$ 418.1242; found: 418.1262 $(M+H)^+$.

4.5. 2-(1,1,1,3,3,3-Hexafluoro-2-hydroxypropan-2-yl)-5-hexylphenanthridin-6(5*H*)-one (11)

The title compound was prepared by a method similar to that described for the synthesis of compound **9**, using 1-iodohexane instead of 2,2,2-trifluoroethyl triflate. White solid. Mp 132.0–132.2 °C. ^{1}H NMR (500 MHz, $CDCl_3$) δ 8.67 (d, J = 1.8 Hz, 1H), 8.54 (d, J = 7.9, 1.8 Hz, 1H), 8.29 (d, J = 7.9 Hz, 1H), 7.84 (d, J = 8.5 Hz, 1H), 7.78 (dd, J = 8.5, 7.3 Hz, 1H), 7.62 (dd, J = 8.5, 7.3 Hz, 1H), 7.46 (d, J = 8.5 Hz, 1H), 4.37 (t, J = 7.9 Hz, 2H), 3.91 (s, 1H), 1.84–1.76 (m, 2H), 1.53–1.47 (m, 2H), 1.42–1.32 (m, 4H), 0.91 (t, J = 7.3 Hz, 3H). HRMS (FAB) calcd for $C_{22}H_{22}F_6NO_2$ 446.1555; found: 446.1516 $(M+H)^+$.

4.6. 2-(1,1,1,3,3,3-Hexafluoro-2-hydroxypropan-2-yl)-5-nonylphenanthridin-6(5*H*)-one (12)

The title compound was prepared by a method similar to that described for the synthesis of compound **9**, using 1-bromononane instead of 2,2,2-trifluoroethyl triflate. White solid. Mp 98.1–99.0 °C. ^{1}H NMR (500 MHz, $CDCl_3$) δ 8.67 (d, J = 1.8 Hz, 1H), 8.54 (d, J = 7.9, 1.8 Hz, 1H), 8.29 (d, J = 7.9 Hz, 1H), 7.84 (d, J = 8.5 Hz, 1H), 7.79 (dd, J = 7.9, 7.3 Hz, 1H), 7.62 (dd, J = 7.9, 7.3 Hz, 1H), 7.46 (d, J = 8.5 Hz, 1H), 4.37 (t, J = 7.9 Hz, 2H), 3.87 (s, 1H), 1.84–1.76 (m, 2H), 1.53–1.46 (m, 2H), 1.43–1.36 (m, 2H), 1.33–1.24 (m, 8H), 0.88 (t, J = 7.3 Hz, 3H). HRMS (FAB) calcd for $C_{25}H_{28}F_6NO_2$ 488.2024; found: 488.1981 $(M+H)^+$.

4.7. 5-Benzyl-2-(1,1,1,3,3,3-hexafluoro-2-hydroxypropan-2-yl)-phenanthridin-6(5*H*)-one (13)

The title compound was prepared by a method similar to that described for the synthesis of compound **9**, using benzyl bromide instead of 2,2,2-trifluoroethyl triflate. White solid. Mp 80.0–80.9 °C. ^{1}H NMR (500 MHz, $CDCl_3$) δ 8.67 (d, J = 1.3 Hz, 1H), 8.63 (d, J = 8.1, 1.3 Hz, 1H), 8.34 (d, J = 8.1 Hz, 1H), 7.84 (td, J = 7.2, 1.3 Hz, 1H), 7.68 (q, J = 8.3 Hz, 2H), 7.38 (d, J = 9.4 Hz, 1H), 7.34–7.23 (m, 5H), 5.66 (s, 2H), 3.63 (s, 1H). HRMS (FAB) calcd for $C_{23}H_{15}F_6NO_2$ 452.1085; found: 452.1057 $(M+H)^+$. Anal. Calcd for $C_{23}H_{15}F_6NO_2 \cdot 1/3\ H_2O$: C, 60.40; H, 3.45; N, 3.06. Found: C, 60.46; H, 3.47; N, 3.08.

4.8. 5-(Cyclohexylmethyl)-2-(1,1,1,3,3,3-hexafluoro-2-hydroxypropan-2-yl)phenanthridin-6(5*H*)-one (14)

The title compound was prepared by a method similar to that described for the synthesis of compound **9**, using cyclohexylmethyl bromide instead of 2,2,2-trifluoroethyl triflate. White solid. Mp 200.9–201.7 °C. ^{1}H NMR (500 MHz, $CDCl_3$) δ 8.67 (d, J = 1.8 Hz, 1H), 8.55 (d, J = 8.5, 1.8 Hz, 1H), 8.30 (d, J = 8.5 Hz, 1H), 7.83 (d, J = 8.5 Hz, 1H), 7.79 (dd, J = 8.5, 7.3 Hz, 1H), 7.62 (dd, J = 8.5, 7.3 Hz, 1H), 7.46 (d, J = 8.5 Hz, 1H), 4.30 (br s, 2H), 3.75 (s, 1H), 1.98–1.88 (m, 1H), 1.76–1.64 (m, 5H), 1.24–1.17 (m, 5H). HRMS (FAB) calcd for $C_{23}H_{22}F_6NO_2$ 458.1555; found: 458.1569 $(M+H)^+$.

4.9. 5-Butylphenanthridin-6(5*H*)-one (15)

The title compound was prepared by a method similar to that described for the synthesis of **9**, using aniline as a starting material, with slight modifications, that is, 1-iodobutane was used in place of 2,2,2-trifluoroethyl triflate. Colorless oil. ^{1}H NMR (500 MHz, $CDCl_3$) δ 8.54 (dd, 1H, J = 7.9, 1.3 Hz), 8.29 (dd, 1H, J = 8.6, 1.3 Hz), 8.27 (d, 1H, J = 8.6 Hz), 7.74 (ddd, 1H, J = 8.0, 7.4, 1.2 Hz), 7.57 (t, 1H, J = 7.4, Hz), 7.53 (ddd, 1H, J = 8.5, 7.4, 1.2 Hz), 7.40 (d, 1H, J = 8.5 Hz), 7.30 (dd, 1H, J = 8.0, 7.4 Hz), 4.38 (t, 2H, J = 7.9, Hz), 1.78 (td, 2H, J = 7.9, 7.3 Hz), 1.52 (sextet, 2H, J = 7.3 Hz), 1.00 (t, 3H, J = 7.3, Hz). HRMS (FAB) calcd for $C_{17}H_{17}NO$ 252.1388; found: 252.1349 $(M+H)^+$.

4.10. 5-Butyl-1-methylphenanthridin-6(5*H*)-one (16)

The title compound was prepared by a method similar to that described for the synthesis of **15**, using 2-iodo-3-methylaniline as a starting material. Benzoyl chloride was used instead of 2-iodobenzoyl chloride. Pale brown oil. ^{1}H NMR (500 MHz, $CDCl_3$) δ 8.64 (d, 1H, J = 8.0 Hz), 8.44 (d, 1H, J = 8.0 Hz), 7.73 (t, 1H, J = 8.0 Hz), 7.59 (t, 1H, J = 8.0 Hz), 7.42 (t, 1H, J = 8.0 Hz), 7.33 (d, 1H, J = 8.0 Hz), 7.17 (d, 1H, J = 8.0 Hz), 4.40 (t, 2H, J = 7.6 Hz), 2.96 (s, 3H), 184–1.77 (m, 2H), 158–1.48 (m, 2H), 1.02 (t, 3H, J = 7.6 Hz). HRMS (FAB) calcd for $C_{18}H_{19}NO$ 266.1545; found: 266.1568 $(M+H)^+$.

4.11. 5-Butyl-2-methylphenanthridin-6(5*H*)-one (17)

The title compound was prepared by a method similar to that described for the synthesis of **15**, using 4-methylaniline as a starting material. 2-Bromobenzoyl chloride was used instead of 2-iodobenzoyl chloride. Colorless oil. ^{1}H NMR (500 MHz, $CDCl_3$) δ 8.55 (dd, 1H, J = 8.0, 1.2 Hz), 8.28 (d, 1H, J = 8.0 Hz), 8.10 (s, 1H), 7.74 (td, 1H, J = 8.0, 1.2 Hz), 7.57 (m, 1H), 7.37–7.30 (d, 1H, J = 7.6 Hz), 4.38 (t, 2H, J = 7.6 Hz), 2.49 (s, 3H), 1.82–1.75 (m, 3H), 1.56–1.48 (m, 2H), 1.01 (t, 3H, J = 7.3 Hz). HRMS (FAB) calcd for $C_{18}H_{19}NO$ 266.1545; found: 266.1584 $(M+H)^+$.

4.12. 5-Butyl-3-methylphenanthridin-6(5*H*)-one (18)

The title compound was prepared by a method similar to that described for the synthesis of **16**, using 2-bromo-5-methylaniline as a starting material. Pale brown oil. ^{1}H NMR (500 MHz, $CDCl_3$) δ 8.53 (d, 1H, J = 8.0 Hz), 8.24 (d, 1H, J = 8.0 Hz), 8.80 (d, 1H, J = 8.0 Hz), 7.73 (t, 1H, J = 8.0 Hz), 7.55 (t, 1H, J = 8.0 Hz), 7.20 (s, 1H), 7.13 (d, 1H, J = 8.0 Hz), 4.39 (t, 2H, J = 7.5 Hz), 2.52 (s, 3H), 1.83–1.76 (m, 2H), 1.57–1.49 (m, 2H), 1.03 (t, 3H, J = 7.5 Hz). HRMS (FAB) calcd for $C_{18}H_{19}NO$ 266.1545; found: 266.1512 $(M+H)^+$.

4.13. 5-Butyl-4-methylphenanthridin-6(5*H*)-one (19)

The title compound was prepared by a method similar to that described for the synthesis of **17**, using 2-methylaniline as a starting material. Colorless oil. ^{1}H NMR (500 MHz, $CDCl_3$) δ 8.50 (dd, 1H, J = 8.0, 1.2 Hz), 8.22 (d, 1H, J = 8.0 Hz), 8.13 (d, 1H, J = 8.0 Hz), 7.20 (td, 1H, J = 7.6, 1.4 Hz), 7.55 (t, 1H, J = 8.0 Hz), 7.30 (d, 1H, J = 7.6 Hz), 7.21 (t, 1H, J = 7.6 Hz), 4.49 (t, 2H, J = 7.6 Hz), 2.66 (s, 3H), 1.66–1.60 (m, 2H), 1.20–1.19 (m, 2H), 0.86 (t, 3H, J = 7.3 Hz). HRMS (FAB) calcd for $C_{18}H_{19}NO$ 266.1545; found: 266.1557 $(M+H)^+$.

4.14. 5-Butyl-7-methylphenanthridin-6(5*H*)-one (20)

The title compound was prepared by a method similar to that described for the synthesis of **16**, using 2-bromoaniline as a starting material. 2-Methylbenzoyl chloride was used instead of benzoyl chloride. White amorphous solid. ^{1}H NMR (500 MHz, $CDCl_3$) δ 8.27 (d, 1H, J = 7.5 Hz), 8.17 (d, 1H, J = 7.5 Hz), 7.58 (t, 1H, J = 7.5 Hz), 7.51 (t, 1H, J = 7.5 Hz), 7.35 (t, 1H, J = 7.5 Hz), 7.26 (t, 1H, J = 7.5 Hz), 4.31 (t, 2H, J = 8.0 Hz), 2.98 (s, 3H), 1.81–1.74 (m, 2H), 1.58–1.49 (m, 2H), 1.02 (t, 3H, J = 7.3 Hz). HRMS (FAB) calcd for $C_{18}H_{19}NO$ 266.1545; found: 266.1573 $(M+H)^+$.

4.15. 5-Butyl-8-methylphenanthridin-6(5*H*)-one (21)

The title compound was prepared by a method similar to that described for the synthesis of **20**. 3-Methylbenzoyl chloride was used instead of 2-methylbenzoyl chloride. White amorphous solid. ^{1}H NMR (500 MHz, $CDCl_3$) δ 8.36 (s, 1H), 8.28 (d, 1H, J = 8.0 Hz), 8.18 (d, 1H, J = 8.0 Hz), 7.58 (dd, 1H, J = 8.0, 1.8 Hz), 7.52 (t, 1H, J = 8.0 Hz), 7.41 (d, 1H, J = 8.0 Hz), 7.30 (t, 1H, J = 8.0 Hz), 4.40 (t, 2H, J = 8.0 Hz), 2.52 (s, 3H), 1.83–1.76 (m, 2H), 1.56–1.50 (m, 2H), 1.02 (t, 3H, J = 7.3 Hz). HRMS (FAB) calcd for $C_{18}H_{19}NO$ 266.1545; found: 266.1588 $(M+H)^+$.

4.16. 5-Butyl-9-methylphenanthridin-6(5*H*)-one (22)

The title compound was prepared by a method similar to that described for the synthesis of **20**. 4-Methylbenzoyl chloride was used instead of 2-methylbenzoyl chloride. White solid. Mp 70.0–73.0 °C. ^{1}H NMR (500 MHz, $CDCl_3$) δ 8.44 (d, 1H, J = 7.5 Hz), 8.30 (d, 1H, J = 7.5 Hz), 8.07 (s, 1H7.5), 7.53 (td, 1H, J = 7.5 Hz), 7.40 (d, 2H, J = 7.5 Hz), 7.30 (dd, 1H, J = 7.5 Hz), 4.39 (t, 2H, J = 8.0 Hz), 2.57 (s, 3H), 1.81.75 (m, 2H), 1.51.49 (m, 2H), 1.02 (t, 3H, J = 7.3 Hz). HRMS (FAB) calcd for $C_{18}H_{19}NO$ 266.1545; found: 266.1527 $(M+H)^+$.

4.17. 5-Butyl-10-methylphenanthridin-6(5*H*)-one (23)

The title compound was prepared by a method similar to that described for the synthesis of **20**. Colorless oil. ^{1}H NMR (500 MHz, $CDCl_3$) δ 8.53 (d, 1H, J = 8.0 Hz), 8.70 (dd, 1H, J = 8.0, 1.2 Hz), 7.61 (d, 1H, J = 8.0 Hz), 7.56–7.52 (m, 1H), 7.49 (d, 1H, J = 8.0 Hz), 7.46 (dd, 1H, J = 8.0, 1.2 Hz), 7.32–7.27 (m, 1H), 4.40 (t, 2H, J = 7.3 Hz), 2.97 (s, 3H), 1.85–1.78 (m, 2H), 1.50–1.50 (m, 2H), 1.02 (t, 3H, J = 7.3 Hz). HRMS (FAB) calcd for $C_{18}H_{19}NO$ 266.1545; found: 266.1553 $(M+H)^+$.

4.18. 5-Butyl-2-fluorophenanthridin-6(5*H*)-one (24)

The title compound was prepared by a method similar to that described for the synthesis of **17**, using 4-fluoroaniline as a starting material. White solid. FAB-MS m/z 270 $(M+H)^+$. Mp 114.0–117.5 °C. ^{1}H NMR (500 MHz, $CDCl_3$) δ 8.56 (dd, 1H, J = 8.0, 1.5 Hz), 8.17 (d, 1H, J = 8.0 Hz), 7.90 (dd, 1H, J = 9.7, 3.0 Hz), 7.77 (t, 1H, J = 8.0 Hz), 7.63 (t, 1H, J = 8.0 Hz), 7.37 (dd, 1H, J = 9.0, 4.5 Hz), 7.29–7.24 (m, 1H), 4.38 (t, 2H, J = 8.0 Hz), 1.82–1.75 (m, 2H), 1.57–1.48 (m, 2H), 1.02 (t, 3H, J = 7.3 Hz). Anal. Calcd for $C_{17}H_{16}NFO$: C, 75.82; H, 5.99; N, 5.20. Found: C, 76.22; H, 6.24; N, 5.24.

4.19. 5-Butyl-2-trifluoromethylphenanthridin-6(5*H*)-one (26)

The title compound was prepared by a method similar to that described for the synthesis of **17**, using 4-trifluoromethylaniline as a starting material. White solid. FAB-MS m/z 320 $(M+H)^+$. Mp 111.0–112.0 °C. ^{1}H NMR (500 MHz, $CDCl_3$) δ 8.56 (d, 1H, J = 8.0 Hz), 8.53 (s, 1H), 8.30 (d, 1H, J = 8.0 Hz), 7.82 (t, 1H, J = 8.0 Hz), 7.77 (dd, 1H, J = 8.0, 1.8 Hz), 7.65 (t, 1H, J = 8.0 Hz), 7.00 (d, 1H, J = 8.0 Hz), 4.41 (t, 2H, J = 7.9 Hz), 1.83–1.75 (m, 2H), 1.58–1.49 (m, 2H), 1.03 (t, 3H, J = 7.3 Hz). Anal. Calcd for $C_{18}H_{16}NF_3O$: C, 67.70; H, 5.05; N, 4.39. Found: C, 67.91; H, 5.33; N, 4.38.

4.20. 5-Butyl-2-ethylphenanthridin-6(5*H*)-one (27)

The title compound was prepared by a method similar to described that for the synthesis of **17**, using 4-ethylaniline as a starting material. Pale brown oil. ^{1}H NMR (500 MHz, $CDCl_3$) δ 8.55 (dd, 1H, J = 8.0, 1.5 Hz), 8.30 (d, 1H, J = 8.0 Hz), 8.12 (d, 1H, J = 1.5 Hz), 7.75 (td, 1H, J = 8.0, 1.5 Hz), 7.58 (t, 1H, J = 8.0 Hz), 7.39 (dd, 1H, J = 8.0, 1.5 Hz), 7.34 (d, 1H, J = 8.0 Hz), 4.39 (t, 2H, J = 8.0 Hz), 2.79 (q, 2H, J = 8.0 Hz), 1.83–1.76 (m, 2H), 1.57–1.49 (m, 2H), 1.34 (t, 3H, J = 7.6 Hz), 1.02 (t, 3H, J = 7.3 Hz). HRMS (FAB) calcd for $C_{19}H_{21}NO$ 280.1701; found: 280.1696 $(M+H)^+$.

4.21. 5-Butyl-2-isopropylphenanthridin-6(5*H*)-one (28)

The title compound was prepared by a method similar to that described for the synthesis of **15**, using 4-isopropylaniline as a starting material. Colorless oil. ^{1}H NMR (500 MHz, $CDCl_3$) δ 8.54 (dd, 1H, J = 8.0, 1.2 Hz), 8.30 (d, 1H, J = 8.0 Hz), 8.12 (d, 1H, J = 1.9 Hz), 7.74 (ddd, 1H, J = 7.9, 7.4, 1.2 Hz), 7.56 (dd, 1H, J = 8.0, 7.4 Hz), 7.41 (dd, 1H, J = 8.6, 1.9 Hz), 7.34 (d, 1H, J = 8.6 Hz), 4.37 (t, 2H, J = 8.0 Hz), 3.05 (septet, 1H, J = 7.4 Hz), 1.77 (quintet, 2H, J = 8.0 Hz), 1.51 (sextet, 2H, J = 7.4 Hz), 1.34 (d, 6H, J = 7.4 Hz), 1.00 (t, 3H, J = 7.4 Hz). HRMS (FAB) calcd for $C_{20}H_{23}NO$ 294.1858; found: 294.1851 $(M+H)^+$.

4.22. 5-Butyl-2-*tert*-butylphenanthridin-6(5*H*)-one (31)

The title compound was prepared by a method similar to that described for the synthesis of **17** using 4-*tert*-burylaniline as a starting material. Pale brown oil. ^{1}H NMR (500 MHz, $CDCl_3$) δ 8.56 (dd, 1H, J = 8.0, 1.5 Hz), 8.32 (d, 1H, J = 8.0 Hz), 8.31 (d, 1H, J = 1.5 Hz), 7.78–7.74 (m, 1H), 7.60 (dd, 1H, J = 8.0, 1.5 Hz), 7.57 (d, 1H, J = 8.0 Hz), 7.37 (d, 1H, J = 8.0 Hz), 4.39 (t, 2H, J = 7.6 Hz), 1.83–1.76 (m, 2H), 1.56–1.50 (m, 2H), 1.44 (s, 9H), 1.02 (t, 3H, J = 7.3 Hz). HRMS (FAB) calcd for $C_{21}H_{25}NO$ 308.2014; found: 308.2008 $(M+H)^+$.

4.23. 5-Butyl-2-hydroxyphenanthridin-6(5*H*)-one (25)

The title compound was prepared by a method similar to that described for the synthesis of **8**, using 4-*tert*-butyldimethylsilyloxyaniline (prepared from *p*-nitrophenol) as a starting material, with slight modifications. 4-*tert*-Butyldimethylsilyloxyaniline was acylated with butyryl chloride in the presence of triethylamine in dichloromethane, and then hydrogenated with lithium aluminum hydride in tetrahydrofuran. Obtained *N*-butylaniline was coupled with 2-iodobenzoyl chloride, and then cyclized in the presence of palladium (II) acetate, tricyclohexylphosphine tetrafluoroborate and potassium carbonate in *N*,*N*-dimethylacetamide. White solid. Mp 187.0–192.0 °C. ^{1}H NMR (500 MHz, $CDCl_3$) δ 8.55 (d, 1H, J = 7.9 Hz), 8.10 (d, 1H, J = 7.9 Hz), 7.78 (d, 1H, J = 2.4 Hz), 7.67 (t, 1H, J = 7.3 Hz), 7.55 (t, 1H, J = 7.3 Hz), 7.28 (d, 1H, J = 9.2 Hz), 7.14 (dd, 1H, J = 9.2, 2.4 Hz), 6.68 (br s, 1H), 4.37 (t, 2H, J = 7.3 Hz), 1.77 (quintet, 2H, J = 7.3 Hz), 1.49 (sextet, 2H, J = 7.3 Hz), 0.97 (t, 3H, J = 7.3 Hz). HRMS (FAB) calcd for $C_{17}H_{17}NO_2$ 268.1338; found: 268.1344 $(M+H)^+$.

4.24. 5-Butyl-2-hydroxymethylphenanthridin-6(5*H*)-one (29)

White solid. FAB-MS m/z 282 $(M+H)^+$. Mp 150.0–153.0 °C. ^{1}H NMR (500 MHz, $CDCl_3$) δ 18.54 (d, 1H, J = 8.0 Hz), 8.28–8.26 (m, 2H), 7.75 (t, 1H, J = 8.0 Hz), 7.59 (t, 1H, J = 8.0, 1.8 Hz), 7.52 (dd, 1H, J = 8.0, 1.8 Hz), 7.36 (d, 1H, J = 8.0 Hz), 4.83 (d, 2H, J = 6.0 Hz), 4.37 (t, 2H, J = 7.5 Hz), 1.99–1.94 (m, 1H), 1.81–1.74 (m, 2H), 1.55–1.48 (m, 2H), 1.01 (t, 3H, J = 7.5 Hz). Anal. Calcd for $C_{18}H_{19}NO_2$: C, 76.84; H, 6.81; N, 4.98. Found: C, 76.94; H, 6.71; N, 5.01.

4.25. 5-Butyl-2-(1′-hydroxyethyl)phenanthridin-6(5*H*)-one (30)

The title compound was prepared by a method similar to that described for the synthesis of **25**, using 1-(4-aminophenyl)ethanol as a starting material. Pale yellow solid. Mp 95.0–99.0 °C. ^{1}H NMR (500 MHz, $CDCl_3$) δ 8.51 (dd, 1H, J = 7.9, 1.2 Hz), 8.23 (d, 1H, J = 8.5 Hz), 8.22 (d, 1H, J = 1.8 Hz), 7.72 (td, 1H, J = 7.3, 1.2 Hz),

7.56 (dd, 1H, J = 7.9, 7.3 Hz), 7.49 (dd, 1H, J = 8.5, 1.8 Hz), 7.29 (d, 1H, J = 8.5 Hz), 5.03 (q, 1H, J = 6.7 Hz), 4.33 (t, 2H, J = 7.9 Hz), 1.74 (quintet, 2H, J = 7.9 Hz), 1.57 (d, 3H, J = 6.7 Hz), 1.49 (sextet, 2H, J = 7.3 Hz), 0.99 (t, 3H, J = 7.3 Hz). HRMS (FAB) calcd for $C_{19}H_{21}NO_2$ 296.1651; found: 296.1661 $(M+H)^+$.

4.26. 5-Butyl-2-acetylphenanthridin-6(5*H*)-one (32)

The title compound was prepared by the same method as described for the synthesis of **30**. The title compound was generated by partial oxidization of the alcoholic hydroxy group at the final cyclization step. White solid. Mp 114.0–118.0 °C. ^{1}H NMR (500 MHz, $CDCl_3$) δ 8.92 (d, 1H, J = 1.8 Hz), 8.53 (d, 1H, J = 7.3 Hz), 8.37 (d, 1H, J = 7.9 Hz), 8.10 (dd, 1H, J = 9.2, 1.8 Hz), 7.79 (t, 1H, J = 7.3 Hz), 7.61 (dd, 1H, J = 7.9, 7.3 Hz), 7.44 (d, 1H, J = 9.2 Hz), 4.39 (t, 2H, J = 7.9 Hz), 2.69 (s, 3H), 1.77 (quintet, 2H, J = 7.9 Hz), 1.52 (sextet, 2H, J = 7.3 Hz), 1.01 (t, 3H, J = 7.3 Hz). HRMS (FAB) calcd for $C_{19}H_{19}NO_2$ 294.1494; found: 294.1501 $(M+H)^+$.

4.27. 5-Butyl-2-phenethylphenanthridin-6(5*H*)-one (33)

Compound **29** was oxidized with manganese oxide in dichloromethane to give an aldehyde derivative, which was coupled by Wittig reaction to give a styryl derivative. This product was hydrogenated in the presence of palladium–carbon under a hydrogen atmosphere to give the title compound. Colorless oil. ^{1}H NMR (500 MHz, $CDCl_3$) δ 8.55 (dd, 1H, J = 8.0, 1.2 Hz), 8.22 (d, 1H, J = 8.0 Hz), 8.05 (s, 1H), 7.74 (ddd, 1H, J = 8.0, 6.5, 1.2 Hz), 7.58 (t, 1H, J = 8.0 Hz), 7.37–7.29 (m, 4H), 7.24–7.21 (m, 3H), 4.38 (t, 2H, J = 7.9 Hz), 3.09–2.99 (m, 4H), 1.82–1.76 (m, 2H), 1.55–1.49 (m, 2H), 1.02 (t, 3H, J = 7.3 Hz). HRMS (FAB) calcd for $C_{25}H_{26}NO$ 356.2014; found: 356.1995 $(M+H)^+$.

4.28. 6-Butyl-8,9,10,11-tetrahydro-8,8,11,11-tetramethylbenzo-[2,3-*b*]phenanthridin-5(6*H*)-one (35)

The title compound was prepared by a method similar to that described for the synthesis of **17**, using 2-amino-5,6,7,8-tetrahydro-5,5,8,8-tetramethylnaphthalene as a starting material. Colorless oil. ^{1}H NMR (500 MHz, $CDCl_3$) δ 8.52 (d, 1H, J = 8.0 Hz), 8.26 (d, 1H, J = 8.0 Hz), 8.21 (s, 1H), 7.73 (t, 1H, J = 8.0 Hz), 7.54 (t, 1H, J = 8.0 Hz), 7.31 (s, 1H), 4.39 (t, 2H, J = 7.3 Hz), 1.84–1.75 (m, 6H), 1.59–1.50 (m, 2H), 1.40 (s, 6H), 1.38 (s, 6H), 1.04 (t, 3H, J = 7.3 Hz). HRMS (FAB) calcd for $C_{25}H_{31}NO$ 362.2484; found: 362.2473 $(M+H)^+$.

4.29. 6-Benzyl-8,9,10,11-tetrahydro-8,8,11,11-tetramethylbenzo-[2,3-*b*]phenanthridin-5(6*H*)-one (36)

The title compound was prepared by a method similar to that described for the synthesis of **35**. N-Alkylation was performed by using benzyl bromide. White amorphous solid. ^{1}H NMR (500 MHz, $CDCl_3$) δ 8.60 (dd, 2H, J = 8.0, 1.5 Hz), 8.29 (d, 1H, J = 8.0 Hz), 8.18 (s, 1H), 7.79–7.75 (m, 1H), 7.58 (t, 1H, J = 8.0 Hz), 7.37–7.28 (m, 4H), 7.23 (s, 1H), 7.22 (t, 1H, J = 8.0 Hz), 5.65 (s, 2H), 1.69 (d, 4H, J = 1.2 Hz), 1.36 (s, 6H), 1.14 (s, 6H). HRMS (FAB) calcd for $C_{28}H_{29}NO$ 396.2327; found: 396.2296 $(M+H)^+$.

4.30. 6-Cyclohexylmethyl-8,9,10,11-tetrahydro-8,8,11,11-tetramethylbenzo[2,3-*b*]phenanthridin-5(6*H*)-one (37)

The title compound was prepared by a method similar to that described for the synthesis of **35**. N-Alkylation was performed by using cyclohexylmethyl bromide. White solid. Mp 148.0–153.0 °C. ^{1}H NMR (500 MHz, $CDCl_3$) δ 8.52 (dd, 2H, J = 8.0, 1.2 Hz), 8.27 (d, 1H, J = 8.0 Hz), 8.21 (s, 1H), 7.73 (td, 1H, J = 8.0, 1.2 Hz), 7.54 (td, 1H, J = 8.0, 1.2 Hz), 7.29 (s, 1H), 4.30 (br s, 2H), 1.94–1.89 (m, 1H), 1.78 (s, 4H), 1.76 (t, 4H, J = 13.00 Hz), 1.41 (s, 6H), 1.38 (s, 6H), 1.29–1.15 (m, 6H). HRMS (FAB) calcd for $C_{28}H_{35}NO$ 402.2797; found: 402.2791 $(M+H)^+$.

4.31. 5-Butyl-8,9,10,11-tetrahydro-8,8,11,11-tetramethylbenzo-[2,3-*j*]phenanthridin-6(5*H*)-one (38)

The title compound was prepared by a method similar to that described for the synthesis of **20**. 5,6,7,8-Tetrahydro-5,5,8,8-tetramethyl-2-naphthoyl chloride (prepared from 5,6,7,8-tetrahydro-5,5,8,8-tetramethylnaphthalene-2-carboxylic acid)[4] was used instead of 2-methylbenzoyl chloride. White solid. FAB-MS m/z 362 $(M+H)^+$. Mp 103.0–109.0 °C. ^{1}H NMR (500 MHz, $CDCl_3$) δ 8.51 (s, 1H), 8.29 (d, 1H, J = 7.9 Hz), 8.21 (s, 1H), 7.50 (t, 1H, J = 7.9 Hz), 7.38 (d, 1H, J = 7.9 Hz), 7.29 (t, 1H, J = 7.3 Hz), 4.38 (t, 2H, J = 7.6 Hz), 1.81–1.74 (m, 6H), 1.56–1.50 (m, 2H), 1.42 (s, 6H), 1.40 (s, 6H), 1.02 (t, 3H, J = 7.3 Hz). Anal. Calcd for $C_{25}H_{31}NO \cdot 1/7\ H_2O$: C, 82.47; H, 8.66; N, 3.85. Found: C, 82.64; H, 8.76; N, 3.71.

4.32. 8,9,10,11-Tetrahydro-8,8,11,11-tetramethylbenzo[2,3-*b*]-phenanthridin-5(6*H*)-one (34)

The title compound was prepared by a method similar to that described for the synthesis of **35**, using 4-methoxybenzyl bromide instead of 1-iodobutane, followed by deprotection of the 4-methoxybenzyl group with trifluoroacetic acid. White solid. Mp 280 °C (decomp). ^{1}H NMR (500 MHz, $CDCl_3$) δ 9.27 (s, 1H), 8.51 (dd, 1H, J = 7.8, 1.3 Hz), 8.28 (t, 1H, J = 7.8 Hz), 8.14 (s, 1H), 7.78 (td, 1H, J = 7.8, 1.3 Hz), 7.57 (t, 1H, J = 7.8 Hz), 7.11 (s, 1H), 1.76 (s, 4H), 1.39 (s, 6H), 1.38 (s, 6H). HRMS (FAB) calcd for $C_{21}H_{23}NO$ 306.1858; found: 306.1817 $(M+H)^+$.

4.33. 6-Butylbenzo[*b*]phenanthridin-5(6*H*)-one (39)

The title compound was prepared by a method similar to that described for the synthesis of **8**, using 2-butylaminonaphthalene as a starting material. 2-Butylaminonaphthalene was prepared from 2-bromonaphthalene by coupling reaction with *n*-butylamine in the presence of tris(dibenzylidenacetone)dipalladium, sodium *tert*-butoxide and n-butylamine. 2-Bromobenzoyl chloride was used instead of 2-iodobenzoyl chloride. White solid. Mp 101.0–104.0 °C. ^{1}H NMR (500 MHz, $CDCl_3$) δ 8.90 (s, 1H), 8.57 (dd, 1H, J = 8.0, 1.8 Hz), 8.46 (d, 1H, J = 8.0 Hz), 7.98 (d, 1H, J = 8.0 Hz), 7.92 (d, 1H, J = 8.0 Hz), 7.82–7.78 (m, 1H), 7.73 (s, 1H), 7.62 (t, 1H, J = 7.3 Hz), 7.55 (t, 1H, J = 7.3 Hz), 7.48 (t, 1H, J = 7.3 Hz), 4.50 (t, 3H, J = 7.9 Hz), 1.92–1.85 (m, 2H), 1.63–1.52 (m, 2H), 1.06 (t, 3H, J = 7.3 Hz). HRMS (FAB) calcd for $C_{21}H_{19}NO$ 302.1545; found: 302.1555 $(M+H)^+$.

4.34. 5-Butylbenzo[*j*]phenanthridin-6(5*H*)-one (40)

The title compound was prepared by a method similar to that described for the synthesis of **20**. 2-Naphthoyl chloride was used instead of 2-methylbenzoyl chloride. White solid. Mp 111.0–115.0 °C. ^{1}H NMR (500 MHz, $CDCl_3$) δ 9.14 (s, 1H), 8.74 (s, 1H), 8.48 (dd, 1H, J = 8.0, 1.5 Hz), 8.09 (d, 1H, J = 8.0 Hz), 8.04 (d, 1H, J = 8.0 Hz), 7.63 (t, 1H, J = 8.0 Hz), 7.57 (d, 1H, J = 8.0 Hz), 7.54 (dd, 1H, J = 8.0, 1.5 Hz), 7.42 (d, 1H, J = 8.0 Hz), 7.35 (t, 1H, J = 8.0 Hz), 4.43 (t, 2H, J = 7.6 Hz), 1.87–1.80 (m, 2H), 1.58–1.52 (m, 2H). HRMS (FAB) calcd for $C_{21}H_{19}NO$ 302.1545; found: 302.1591 $(M+H)^+$.

4.35. 5-Butylbenzo[*c*]phenanthridin-6(5*H*)-one (41)

The title compound was prepared by a method similar to that described for the synthesis of **17**, using 1-aminonaphthlene as a

starting material. White amorphous solid. ^{1}H NMR (500 MHz, $CDCl_3$) δ 8.55 (dd, 1H, J = 8.0, 1.2 Hz), 8.29–8.22 (m, 3H), 7.92–7.89 (m, 1H), 7.81–7.77 (m, 1H), 7.73 (d, 1H, J = 8.0 Hz), 7.60 (t, 3H, J = 8.0 Hz), 7.56–7.50 (m, 2H), 4.59 (t, 2H, J = 7.3 Hz), 1.93–1.86 (m, 2H), 1.26–1.18 (m, 2H), 0.83 (t, 3H, J = 7.3 Hz). HRMS (FAB) calcd for $C_{21}H_{19}NO$ 302.1545; found: 302.1574 $(M+H)^+$.

4.36. 6-Butylbenzo[*a*]phenanthridin-5(6*H*)-one (42)

The title compound was prepared by the same method as described for the synthesis of **39**. The title compound was fractionated by means of HPLC. Colorless oil. ^{1}H NMR (500 MHz, $CDCl_3$) δ 8.80 (d, 1H, J = 8.5 Hz), 8.68 (d, 1H, J = 8.5 Hz), 8.64 (dd, 1H, J = 8.5, 1.5 Hz), 7.95 (t, 2H, J = 8.5 Hz), 7.79 (td, 1H, J = 8.5, 1.5 Hz), 7.65–7.60 (m, 3H), 7.52 (t, 1H, J = 8.5 Hz), 4.50 (t, 2H, J = 7.5 Hz), 1.88–1.80 (m, 2H), 1.58–1.53 (m, 2H), 1.03 (t, 3H, J = 7.3 Hz). HRMS (FAB) calcd for $C_{21}H_{19}NO$ 302.1545; found: 302.1534 $(M+H)^+$.

4.37. 5-Butylbenzo[*k*]phenanthridin-6(5*H*)-one (43)

The title compound was prepared by the same method as described for the synthesis of **40**. The title compound was fractionated by means of HPLC. White solid. Mp 54.0–60.0 °C. ^{1}H NMR (500 MHz, $CDCl_3$) δ 8.88 (d, 1H, J = 7.3 Hz), 8.66 (d, 1H, J = 8.5 Hz), 8.51 (d, 1H, J = 8.5 Hz), 8.01 (dd, 2H, J = 7.3, 3.0 Hz), 7.95 (d, 1H, J = 8.5 Hz), 7.70–7.63 (m, 3H), 7.59 (t, 1H, J = 7.3 Hz), 7.53 (d, 2H, J = 8.5 Hz), 7.36 (t, 2H, J = 8.5 Hz), 4.45 (t, 2H, J = 7.9 Hz), 1.90–1.83 (m, 3H), 1.57–1.51 (m, 2H), 1.03 (t, 3H, J = 7.5 Hz). HRMS (FAB) calcd for $C_{21}H_{19}NO$ 302.1545; found: 302.1567 $(M+H)^+$.

4.38. 6-Butylbenzo[*i*]phenanthridin-5(6*H*)-one (44)

The title compound was prepared by a method similar to that described for the synthesis of **40**. 1-Naphthoyl chloride was used instead of 2-naphthoyl chloride. White amorpous solid. ^{1}H NMR (500 MHz, $CDCl_3$) δ 10.30 (d, 1H, J = 9.0 Hz), 8.44 (dd, 1H, J = 8.0, 1.2 Hz), 8.39 (d, 1H, J = 9.0 Hz), 8n.17 (d, 1H, J = 9.0 Hz), 7.94 (dd, 1H, J = 8.0, 1.2 Hz), 7.77–7.73 (m, 1H), 7.65–7.60 (m, 2H), 7.49 (d, 1H, J = 8.0 Hz), 7.36 (t, 1H, J = 8.0 Hz), 4.50 (t, 2H, J = 7.6 Hz), 1.90–1.83 (m, 2H), 1.63–1.53 (m, 2H), 1.06 (t, 3H, J = 7.3 Hz). HRMS (FAB) calcd for $C_{21}H_{19}NO$ 302.1545; found: 302.1540 $(M+H)^+$.

4.39. Bioassay

NNC #2 cells carrying full-genomic HCV RNA replicons were maintained in high-glucose Dulbecco's modified Eagle's medium (DMEM) in the presence of 10% (v/v) fetal bovine serum (FBS) and 1 mg/mL G418 (Sigma). Cells at 70% confluence were collected after treatment with trypsin and resuspended in the same medium (5×10^4 cells/mL). One hundred microliters of the cell suspension was transferred to each well of a 96-well plate and cultured at 37 °C for 24 h. Then the medium was removed, and 200 μL of DMEM supplemented with 10% FBS containing various concentrations of test compound was added to each well. After incubation for 3 days, the cells were treated with lysis buffer of a TaqMan Gene Expression Cell-to-CT™ Kit. Expression levels of HCV RNA and GAPDH RNA were measured with the kit, according to the manufacturer's instructions. The RNA levels were quantified by real-time RT-PCR using an ABI 7500 Real-Time PCR System (Applied Biosystems). The anti-HCV activity and cytotoxicity of test compounds were expressed as EC_{50} and CC_{50} determined from the decrease of HCV RNA and GAPDH RNA levels, respectively, as described above.

Acknowledgments

The work described in this paper was partially supported by Grants-in Aid for Scientific Research from the Science and Technology Incubation Program in Advanced Regions, Japan Science and Technology Agency (JST), Japan and The Ministry of Education, Culture, Sports, Science and Technology, Japan, and a Grant from the Japan Society for the Promotion of Science.

References and notes

1. Hashimoto, Y. *Arch. Pharm. Life Sci.* **2008**, *341*, 536.
2. Hosoda, S.; Matsuda, D.; Tomoda, H.; Hashimoto, Y. *Mini-Rev. Med. Chem.* **2009**, *9*, 572.
3. Hosoda, S.; Aoyama, H.; Goto, Y.; Salim, M. T. A.; Okamoto, M.; Hashimoto, M.; Baba, M.; Hashimoto, Y. *Bioorg. Med. Chem. Lett.* **2009**, *19*, 3157.
4. Nakamura, M.; Hamasaki, T.; Tokitou, M.; Baba, M.; Hashimoto, Y.; Aoyama, H. *Bioorg. Med. Chem.* **2009**, *17*, 4740.
5. Hosoda, S.; Matsuda, D.; Tomoda, H.; Hashimoto, M.; Aoyama, H.; Hashimoto, Y. *Bioorg. Med. Chem. Lett.* **2009**, *19*, 4228.
6. Koonin, E. V.; Wolf, Y. I.; Karev, G. P. *Nature* **2002**, *420*, 218.
7. Grishin, N. V. *J. Struct. Biol.* **2001**, *134*, 167.
8. Koch, M. A.; Wittenberg, L.-O.; Basu, S.; Jeyaraj, D. A.; Gourzoulidou, E.; Reinecke, K.; Odermatt, A.; Waldmann, H. *Proc. Natl. Acad. Sci. U.S.A.* **2004**, *101*, 16721.
9. Hashimoto, Y. *Curr. Med. Chem.* **1998**, *5*, 163.
10. Hashimoto, Y. *Bioorg. Med. Chem.* **2002**, *10*, 461.
11. Hashimoto, Y. *Mini-Rev. Med. Chem.* **2002**, *2*, 543.
12. Hashimoto, Y.; Tanatani, A.; Nagasawa, K.; Miyachi, H. *Drugs Future* **2004**, *29*, 383.
13. Hashimoto, Y. *Cell Biol. Rev.* **1991**, *25*, 209.
14. Sako, K.; Aoyama, H.; Sato, S.; Hashimoto, Y.; Baba, M. *Bioorg. Med. Chem.* **2008**, *16*, 3780.
15. Aoyama, H.; Sako, K.; Sato, S.; Nakamura, M.; Miyachi, H.; Baba, M.; Hashimoto, Y. *Heterocycles* **2009**, *77*, 779.
16. Liang, T. J.; Rehermann, B.; Seeff, L. B.; Hoofnagle, J. H. *Ann. Intern. Med.* **2000**, *132*, 296.
17. Hayashi, P. H.; Di Bisceglie, A. M. *Med. Clin. North Am.* **2005**, *89*, 371.
18. Memon, M. I.; Memon, M. A. *J. Viral Hepat.* **2002**, *9*, 84.
19. Echevarria-Mayo, J. M. *Enferm. Infecc. Microbiol. Clin.* **2006**, *24*, 45.
20. Bosch, F. X.; Ribes, J.; Cleries, R.; Diaz, M. *Clin. Liver Dis.* **2005**, *9*, 191.
21. McHutchison, J. G.; Gordon, S. C.; Schiff, E. R.; Shiffman, M. L.; Lee, W. M.; Rustgi, V. K.; Goodman, Z. D.; Ling, M. H.; Cort, S.; Albrecht, J. K. *N. Eng. J. Med.* **1998**, *339*, 1485.
22. Tan, S. L.; Pause, A.; Shi, Y.; Sonenberg, N. *Nat. Rev. Drug Disc.* **2002**, *1*, 867.
23. Buckwold, V. E.; Beer, B. E.; Donis, R. O. *Antiviral Res.* **2003**, *60*, 1.
24. Buckwold, V. E.; Wei, J.; Wenzel-Mathers, M.; Russell, J. *Antimicrob. Agents Chemother.* **2003**, *47*, 2293.
25. Yanagida, K.; Baba, C.; Baba, M. *Antiviral Res.* **2004**, *64*, 195.
26. Aoyama, A.; Aoyama, H.; Dodo, K.; Makishima, M.; Hashimoto, Y.; Miyachi, H. *Heterocycles* **2008**, *76*, 137.
27. Miyachi, H.; Aoyama, A.; Hashimoto, Y. *MedChemNews* **2009**, *19*(2), 30.
28. Ishii, N.; Watashi, K.; Hishiki, T.; Goto, K.; Inoue, D.; Hijikata, M.; Wakita, T.; Kato, N.; Shimotohno, K. *J. Virol.* **2006**, *80*, 4510.
29. Li, L.; Liu, J.; Zhu, L.; Cutler, S.; Hasegawa, H.; Shan, B.; Medina, J. C. *Bioorg. Med. Chem. Lett.* **2006**, *16*, 1638.

Antiviral Research 88 (2010) 263–268

Contents lists available at ScienceDirect

Antiviral Research

journal homepage: www.elsevier.com/locate/antiviral

Highly potent and selective inhibition of bovine viral diarrhea virus replication by γ-carboline derivatives

Mohammed T.A. Salim[a], Yukinori Goto[a,1], Takayuki Hamasaki[a], Mika Okamoto[a], Hiroshi Aoyama[b], Yuichi Hashimoto[b], Simone Musiu[c], Jan Paeshuyse[c], Johan Neyts[c], Matheus Froeyen[c], Piet Herdewijn[c], Masanori Baba[a,*]

[a] Division of Antiviral Chemotherapy, Center for Chronic Viral Diseases, Graduate School of Medical and Dental Sciences, 8-35-1, Sakuragaoka, Kagoshima University, Kagoshima, 890-8544, Japan
[b] Institute of Molecular and Cellular Biosciences, The University of Tokyo, Tokyo 113-0032, Japan
[c] Rega Institute for Medical Research, Katholieke Universiteit Leuven, B-3000 Leuven, Belgium

ARTICLE INFO

Article history:
Received 10 June 2010
Received in revised form
10 September 2010
Accepted 17 September 2010

Keywords:
Flavivirus
BVDV
HCV
Carboline
RNA polymerase
Drug-resistance

ABSTRACT

Several novel γ-carboline derivatives were identified as selective inhibitors of bovine viral diarrhea virus (BVDV) replication in cell cultures. Among them, 3,4,5-trimethyl-γ-carboline (SK3M4M5M) was the most active against BVDV (Nose strain) in MDBK cells, with a 50% effective concentration of 0.017 ± 0.005 μM and a selectivity index of 435. The compound inhibited viral RNA synthesis in a dose-dependent fashion. In a time of drug-addition experiment during a single viral replication cycle, SK3M4M5M lost its antiviral activity when first added at 8 h or later after infection, which coincides with the onset of viral RNA synthesis. When selected γ-carboline derivatives, including SK3M4M5M, were examined for their inhibitory effect on the mutant strains resistant to some classes of nonnucleoside BVDV RNA-dependent RNA polymerase inhibitors, all of which target the top of the finger domain of the polymerase, the strains displayed cross-resistance to the γ-carboline derivatives. These results indicate that the γ-carboline derivatives may possibly target a hot spot of the RNA-dependent RNA polymerase. Although SK3M4M5M was highly active against BVDV, the compound proved inactive against hepatitis C virus (HCV) in HCV RNA replicon cells.

1. Introduction

Bovine viral diarrhea virus (BVDV), a member of the *pestivirus* genus from the family *Flaviviridae*, causes serious health problems in cattle, which results in great economical loss (Houe, 2003). BVDV infection induces a variety of clinical symptoms, such as respiratory problems, chronic wasting disease, immune system dysfunction, and predisposition to secondary microbial infections. In addition, BVDV infects the fetus by crossing the placenta. Depending on the time of gestation, the infection can result in the birth of a persistently infected calf (Kobrak and Weber, 1997). Two biotypes, namely, non-cytopathic and cytopathic strains can be distinguished. Only non-cytopathic strains have been isolated from persistently infected animals, which are immunotolerant to the virus and are shedding infectious virions in all secretions. The superinfection of a persistently infected animal with a cytopathic strain causes a fatal mucosal disease.

Vaccines are available in some countries in an attempt to control the diseases caused by BVDV (van Oirschot et al., 1999). However, the existence of considerable genetic and antigenic diversity of BVDV is a major concern for the development and efficacy of current vaccines (Kalaycioglu, 2007). An alternative approach could be the use of antiviral agents. Several compounds have recently been identified as selective inhibitors of BVDV replication in cell cultures. These include VP32947 (Baginski et al., 2000), mizoribine (Yanagida et al., 2004), BPIP (Paeshuyse et al., 2006), Acridones (Tabarrini et al., 2006), AG110 (Paeshuyse et al., 2007), SC-560 (Okamoto et al., 2009), iminosugar derivatives (Chang et al., 2009), LZ37 (Paeshuyse et al., 2009), and BIT225 (Luscombe et al., 2010).

We have previously established a simple and sensitive colorimetric assay of compounds for evaluating their antiviral activity against BVDV in cell cultures (Baba et al., 2005). The assay is based on spectrophotometrical assessment of the viability of the cells infected with a cytopathic strain of BVDV by measuring extracellular leakage of lactic dehydrogenase (LDH). Using this system, we screened a number of small molecules for their inhibitory effect on BVDV replication in cell cultures. Among them, some γ-carboline derivatives were identified as highly potent and selective inhibitors of BVDV. In particular, dimethyl- and trimethyl-γ-carbolines could

* Corresponding author. Tel.: +81 99 275 5930; fax: +81 99 275 5932.
E-mail address: m-baba@vanilla.ocn.ne.jp (M. Baba).
[1] Present address: Department of Molecular Virology, Research Institute for Microbial Diseases, Osaka University, Suita 565-0871, Japan.

0166-3542/$ – see front matter © 2010 Elsevier B.V. All rights reserved.
doi:10.1016/j.antiviral.2010.09.013

exert their anti-BVDV activity in the nanomolar range (Sako et al., 2008; Aoyama et al., 2009). In this study, we evaluated selected γ-carbolines for their inhibitory effect on the replication of mutant strains resistant to other anti-BVDV agents.

2. Materials and methods

2.1. Compounds

Seven γ-carboline derivatives were used in this study. Their chemical structures are shown in Fig. 1. The synthesis of these compounds has been described previously (Sako et al., 2008; Aoyama et al., 2009). The nonnucleoside BVDV NS5B inhibitors AG110 (Paeshuyse et al., 2007), LZ37 (Paeshuyse et al., 2009), and BPIP (Paeshuyse et al., 2006) were also used in this study (Fig. 1).

2.2. Cells and viruses

Madin-Darby bovine kidney (MDBK) cells were purchased from Japan Health Sciences Foundation (Health Science Research Resources Bank, Osaka, Japan). The cells were grown and maintained in Dulbecco's modified Eagle medium with high glucose (Gibco/BRL, Grand Island, NY). The medium was supplemented with 10% heat-inactivated horse serum (Gibco/BRL), 100 unit/ml penicillin G, and 100 μg/ml streptomycin. The cells were certified as BVDV-contamination negative. For antiviral assays, the medium supplemented with 3% heat-inactivated horse serum and antibiotics was used. The cytopathic BVDV strain Nose was obtained from Kyoto Biken (Kyoto, Japan). The virus was obtained from culture supernatants of infected cells after incubation for 3 days. Virus stocks were stored at −80 °C until use. Their infectivity was determined in MDBK cells by an end point serial dilution method and expressed as 50% cell culture infectious dose per ml ($CCID_{50}$/ml). In addition, three drug-resistant mutant strains and the corresponding wild-type strain NADL were employed (Paeshuyse et al., 2006, 2007, 2009). The strains carry mutations F224S, F224Y, and F291G, and are resistant to BPIP, LZ37, and AG110, respectively. In experiments using these strains, MDBK cells were grown in Eagle's medium supplemented with 5% heat-inactivated fetal bovine serum (Integro, Zaandam, The Netherlands), which proved to be BVDV contamination-free by reverse transcription polymerase chain reaction (RT-PCR).

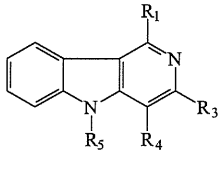

γ-Carboline derivatives

Compound	R_1	R_3	R_4	R_5
γ-Carboline	H	H	H	H
SK5M	H	H	H	CH_3
SK3M4M	H	CH_3	CH_3	H
SK3M5M	H	CH_3	H	CH_3
SK4M5M	H	H	CH_3	CH_3
SK1M4M5M	CH_3	H	CH_3	CH_3
SK3M4M5M	H	CH_3	CH_3	CH_3

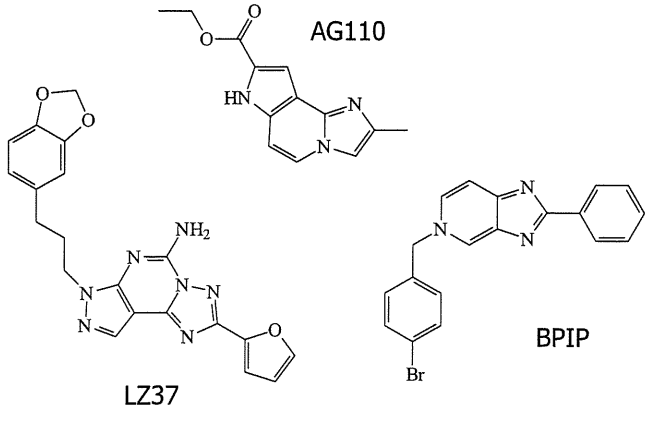

Fig. 1. Chemical structures of γ-carboline derivatives and BVDV RNA-dependent RNA polymerase inhibitors.

2.3. Anti-BVDV assays

Determination of γ-carboline derivatives for their anti-BVDV activity was based on the inhibition of virus-induced cytopathicity in MDBK cells, as previously described (Baba et al., 2005). Briefly, the cells (1×10^5 cells/ml) were infected with BVDV (Nose strain) at a multiplicity of infection (MOI) of 0.01, and 100 μl of the cell suspension was brought into each well in a microtiter plate. The cells were incubated in the presence of various concentrations of the test compounds for 3 days at 37 °C. After incubation, culture supernatants were collected to determine their LDH levels by an LDH detection kit (Takara Biochemicals, Otsu, Japan), according to the manufacturer's instructions. The cytotoxicity of compounds was evaluated in parallel with their antiviral activity. The mock-infected MDBK cells (1×10^4 cell/well) were incubated in the presence of various concentrations of test compounds for 3 days. The viability was determined by a dye method using the water soluble tetrazolium Tetracolor One® (Seikagaku Corporation, Tokyo, Japan).

Antiviral assays using the drug-resistant strains were carried out according to the procedures, as previously described (Paeshuyse et al., 2009). MDBK cells (5×10^3 cells/100 μl) were seeded in a microtiter plate. After incubation for 24 h at 37 °C, culture medium was removed. Serial dilutions of the test compounds were added into each well, and then the cells were infected with the virus at a MOI of 2.0. After 3 days, culture medium was removed, and the virus-induced cytopathicity was quantified by the 3-(4,5-dimethylthiazol-2-yl)-5-(3-carboxymethoxyphenyl)-2-(4-sulfophenyl)-2*H*-tetra-zolium/phenazinemethosulfate (MTS/PMS) method. The cytotoxicity of compounds was also evaluated by the MTS/PMS method in the mock-infected MDBK cells.

2.4. Virus yield reduction assay

MDBK cells (1×10^5/ml) were infected with BVDV (Nose strain) at a MOI of 1.0 and seeded into a 48-well plate in the presence or absence of various concentrations of SK3M4M5M or SK5M. After incubation for 4 h at 37 °C, the cells were washed twice with phosphate-buffered saline (PBS) and incubated with fresh culture medium containing appropriate concentrations of the test compounds. The cells were further incubated for 3 days. Then, the culture supernatants were collected and examined for their virus titer by the end-point dilution method. The virus titer was expressed as $CCID_{50}$/ml.

2.5. RT-PCR

Inhibitory effect of 3,4,5-trimethyl-γ-carboline (SK3M4M5 M) on viral RNA synthesis was determined by real-time RT-PCR. MDBK cells (2×10^4 cells/well) were infected with BVDV (Nose strain) at a MOI of 2.0 and cultured in the presence of various concentrations of the compound. After incubation for 12 h, the cells were washed with PBS, treated with lysis buffer of TaqMan® Gene Expression Cell-to-CT™ kit (Applied Biosystems, Branchburg, NJ), and subjected to real-time RT-PCR. The BVDV RNA level was determined using the sense primer 5′-TGGTCCGACGCCTTAGTATAAAGG-3′, the antisense primer 5′-GGCTGTATTCGTAACAGTTGGTTAAA-3′, and the fluorescence probe 5′-ACGAGGGCACGCCCAAAGCA-3′ (Applied Biosystems). The primer pair amplifies the 5′-untranslated region

of BVDV RNA. RT and PCR reagents of the kit were used for real-time RT-PCR, according to the manufacturer's instructions. Nonspecific inhibition of host cellular mRNA synthesis by the compound was determined by amplification of part of the bovine β-actin RNA using the sense primer (Applied Biosystems).

2.6. Time of drug-addition experiment

MDBK cells (2×10^4 cells/well) were seeded in a 96-well plate and incubated at 37 °C for 24 h. Then, the cells were infected with BVDV (Nose strain) at a MOI of 2.0. After incubation for 1 h, the inoculum was removed, and the cells were washed three times with PBS. SK3M4M5M (1 μM) or BPIP (2 μM) was added at the time of infection and incubated without their removal or added at different time points after infection. The cells were further incubated until 24 h after virus infection. The cells thoroughly washed with PBS and subjected to real-time RT-PCR, as described above.

2.7. Molecular modeling

The published X-ray structure of the BVDV RNA-dependent RNA polymerase [PDB entry 1S48 (Choi et al., 2004)] was used in all docking experiments. Selenium atoms in the selenomethionine residues were modified back to sulphur atoms to get methionine residues. The inhibitor γ-carboline was drawn using Prodrg (Schuettelkopf and van Aalten, 2010). Polar hydrogen atoms and Gasteiger charges were added to the enzyme and inhibitor structures using autodock tools (Mohamadi et al., 1990). γ-Carboline was docked in the cavity in which F224 is located by means of a Lamarckian genetic algorithm and empirical binding free energy (Morris et al., 1998). Interactions (hydrogen bonds and hydrophobic interactions) were calculated using Ligplot (Wallace et al., 1995).

2.8. Anti-HCV assay

The anti-HCV activity of γ-carboline derivatives was determined by the inhibition of viral RNA synthesis in full-genomic HCV RNA replicon cells by real-time RT-PCR, as previously described (Ishii et al., 2006; Watashi et al., 2003). The replicon cells NNC#2 were kindly provided by Dr. Hijikata (Kyoto University, Kyoto, Japan).

3. Results

3.1. Anti-BVDV activity

We demonstrated earlier that the introduction of a methyl group into γ-carboline enhanced its anti-BVDV activity (Sako et al., 2008). This enhancement was found to be stronger, when more methyl groups were introduced into the molecule (Aoyama et al., 2009). In fact, when the selected methyl-γ-carbolines were examined for their inhibitory effect on BVDV (Nose strain) replication in MDBK cells, the highest activity was achieved by SK3M4M5M followed by 4′,5′-dimethyl-γ-carboline (SK4M5M) (Table 1). The 50% effective concentrations (EC_{50}) of SK3M4M5M and SK4M5M were 0.017 ± 0.005 and 0.057 ± 0.005 μM, respectively. Thus, SK3M4M5M and SK4M5M were approximately 147 and 44-fold more potent than their parental compound γ-carboline (EC_{50}: 2.5 ± 0.3 μM) in inhibiting BVDV replication. Although their cytotoxicity was also higher than γ-carboline, the selectivity indices (SI), based on the ratio of 50% cytotoxic concentration (CC_{50}) to EC_{50}, of SK3M4M5M and SK4M5M were 436 and 174, respectively (Table 1), which were approximately 30 and 12-fold greater than the SI of γ-carboline (14.7). The much higher activity of SK3M4M5M, as compared to SK5M, was also confirmed by a virus yield reduction assay. On average, 1.2 and 4.2 log reduction of virus titer in the culture supernatants was recorded in the presence of SK3M4M5M at 0.2 and 1 μM, respectively (Fig. 2). By contrast, little reduction of virus titer was achieved by SK5M even at a concentration of 1 μM.

Table 1
Antiviral activity of γ-carboline derivatives against BVDV (Nose strain) in MDBK cells.

Compound	EC_{50} (μM)	CC_{50} (μM)	SI
γ-Carboline	2.5 ± 0.3	36.7 ± 3.8	15
SK5M	0.36 ± 0.03	22.6 ± 2.7	63
SK3M4M	0.27 ± 0.11	14.5 ± 0.7	54
SK3M5M	0.26 ± 0.04	17.7 ± 1.9	68
SK4M5M	0.057 ± 0.005	9.9 ± 0.7	174
SK1M4M5M	0.14 ± 0.03	1.9 ± 0.1	14
SK3M4M5M	0.017 ± 0.005	7.4 ± 0.9	435

EC_{50}: 50% effective concentration, based on the inhibition of virus-induced cytopathicity; CC_{50}: 50% cytotoxic concentration, based on the reduction of viable cell number; SI: selectivity index, a ratio of CC_{50} to EC_{50}. All data represent means ± SD for three independent experiments.

3.2. Inhibition of viral RNA synthesis and time-of-drug-addition studies

To determine whether SK3M4M5M inhibits BVDV RNA synthesis without affecting host cellular mRNA synthesis, the intracellular RNA levels of BVDV and β-actin were quantified by real-time RT-PCR. As shown in Fig. 3, SK3M4M5M completely inhibited BVDV RNA synthesis at a concentration of 0.1 μM, whereas no inhibition of β-actin RNA synthesis was observed up to 0.1 μM. In addition, viral RNA synthesis was also strongly inhibited by SK3M4M5M at a concentration of 0.1 μM in the cells infected with non-cytopathic strains of BVDV. Its EC_{50} values were 0.034 ± 0.018 and 0.020 ± 0.005 μM for Pe515 and Os Loss strains, respectively (data not shown).

To gain further insight into the mechanism of action, a time-of-drug-addition experiment was conducted. In this experiment, BVDV RNA levels were determined at different time points of drug-addition to the infected cells. SK3M4M5M was used at a concentration of 1.0 μM, which was 10-fold higher than the concentration that completely inhibited BVDV RNA synthesis (Fig. 3). The compound could retain its full activity against BVDV, when

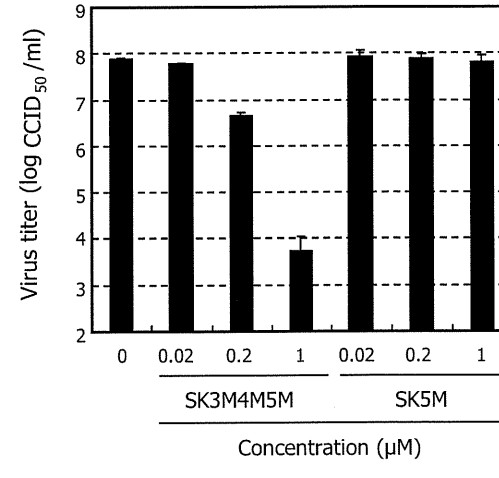

Fig. 2. Inhibitory effect of SM3M4M5M and SK5M on virus production in MDBK cells. The cells were infected with BVDV at a MOI of 1.0 and cultured in the presence or absence of various concentrations of SK3M4M5M or γ-carboline. After incubation for 4 h, the cells were washed with PBS and further incubated with fresh culture medium containing appropriate concentrations of the test compounds. After 3 days, the culture supernatants were collected and examined for their virus titer. The virus titer was expressed as log CCID50/ml. Experiments were repeated three times, and means ± SD are shown.

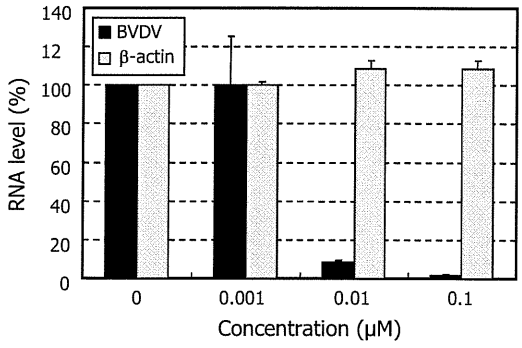

Fig. 3. Effect of SK3M4M5M on BVDV RNA synthesis in MDBK cells. The cells were infected with BVDV at a MOI of 2.0 and cultured in the presence of various concentrations of the compound. After incubation for 12 h, the cells were washed with PBS, treated with lysis buffer and subjected to real-time RT-PCR (see Section 2). Black and gray columns indicate the amounts of BVDV RNA and β-actin RNA, respectively. Data represent means ± SD for triplicate experiments. Experiments were repeated three times, and a representative result is shown.

added during the first 8 h post-infection (Fig. 4A). When the compound was added at a time point later than 8 h after infection, the antiviral activity was lost, and the intracellular viral RNA gradually increased with increasing the time of delayed addition. These results suggest that SK3M4M5M inhibits an event occurring around 8 h after virus infection. Furthermore, an almost identical result was obtained in the experiment with the BVDV RNA polymerase inhibitor BPIP (Fig. 4B). It has been reported that a single cycle of BVDV replication takes 13 h on average and that viral RNA synthesis starts at about 6–8 h after infection (Paeshuyse et al., 2006). Thus, SK3M4M5M appears to interact with a stage in the viral replication cycle that coincides with the onset of viral RNA synthesis.

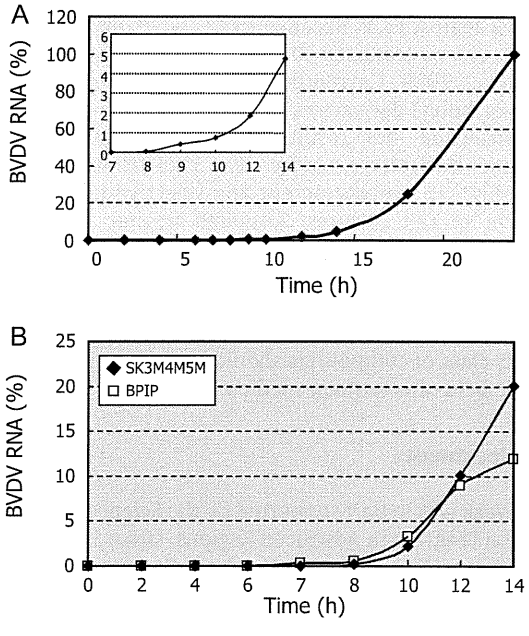

Fig. 4. Effect of time of drug-addition on the antiviral activity of SK3M4M5M. MDBK cells infected with BVDV at a MOI of 2.0. After incubation for 1 h, the inoculum was removed. SK3M4M5M (1 μM) or BPIP (2 μM) was added at the time of infection and incubated without removal of the compound (0 h), or the compound was added at different time points after infection. (A) The cells were further incubated with SK3M4M5M until 24 h after virus infection and subjected to real-time RT-PCR. (B) The cells were further incubated with SK3M4M5 M (filled diamond) or BPIP (open square) up to 24 h after virus infection. Values are expressed as percentage viral RNA of the infected cells untreated with the compound. All data represent means for triplicate experiments. Experiments were repeated twice, and a representative result is shown.

3.3. Activity against NS5B inhibitor-resistant mutants

The antiviral activity of γ-carboline, SK4M5M, SK1M4M5M, and SK3M4M5M was evaluated against three BVDV drug-resistant strains that carry the respective mutations F224S, F224Y, and F291G, which display resistance to BPIP, LZ37, and AG110, respectively. All three molecules have been shown to target the top of the finger domain of the pestivirus RNA polymerase. SK4M5M, and SK1M4M5M, as well as γ-carboline, proved inactive against these mutant strains (Table 2). Interestingly, although SK3M4M5M exhibited reduced activity against the mutant strains, the compound retained overall substantial antiviral activity. Furthermore, the activity of SK3M4M5M against the wild-type of NADL strain was less pronounced than against the Nose strain; however, the anti-BVDV activity was comparable to that of BPIP, which has been reported to be one of the most potent anti-BVDV agents reported so far (Paeshuyse et al., 2006).

3.4. Docking of γ-carboline in the BVDV RNA polymerase crystal structure

The amino acid F224 is located near the tip of the finger domain of the BVDV polymerase. Docking of γ-carboline in this cavity revealed possible interactions between the polymerase and γ-carboline. The following possible interactions were calculated: (i) hydrophobic contacts of γ-carboline with T259, I261 and G223 (Fig. 5A blue shade and Fig. 5B), (ii) a hydrogen bond between the N3 of γ-carboline and the side chain of A392 (Fig. 5A and B), and (iii) aromatic ring stacking interactions between F224 and γ-carboline (Fig. 5A).

3.5. Anti-HCV activity

The γ-carboline derivatives were also examined for their inhibitory effect on HCV replication in replicon cells. However, none of the compounds displayed selective inhibition of HCV replication (data not shown).

4. Discussion

We recently reported two different series of compounds that had selective anti-BVDV activity in cell cultures. One is γ-carboline derivatives, and the other is diphenylmethane derivatives (Sako et al., 2008; Aoyama et al., 2009; Salim et al., 2010). Among them, dimethyl- and trimethyl-γ-carbolines proved to be highly potent and selective inhibitors of BVDV replication (Table 1) (Aoyama et al., 2009). The most potent analogue in this series SK3M4M5M was able to completely inhibit viral RNA synthesis in a single replication cycle assay at a concentration of 100 nM. From a time-of-drug-addition experiment, it appeared that the compound interfered with a step that coincides with the onset of viral RNA synthesis in the replication cycle (Paeshuyse et al., 2009).

Cross-resistance between, two different classes of molecules provides an indirect proof that both have the same molecular target in the viral replication cycle. Therefore, γ-carboline derivatives were examined for their inhibitory effect on the replication of three strains of BVDV that were previously shown to confer resistance to various classes of nonnucleoside NS5B inhibitors (Paeshuyse et al., 2006, 2007, 2009). The antiviral activity of γ-carboline derivatives against the wild-type of NADL strain was several-fold lower than that against the wild-type of Nose strain (Tables 1 and 2). Furthermore, such difference was also observed for their CC_{50} values. This may be attributed to the difference of viral strains and assay conditions used for the experiments, including cytotoxicity evaluation. All of the resistant mutants were less susceptible to the γ-carboline derivatives than the wild-type virus, suggesting that

Table 2
Antiviral activity of γ-carboline derivatives against drug-resistant BVDV in MDBK cells.

Compound	EC_{50} (μM)				CC_{50} (μM)
	WT (NADL strain)	F224S	F224Y	E291G	
γ-Carboline	28.2 ± 9.0	>88.1	>88.1	>88.1	88.1 ± 5.0
SK4M5M	0.38 ± 0.31	>16.7	3.1 ± 0.8	>16.7	16.7 ± 0.7
SK1M4M5M	0.98 ± 0.09	>3.7	>3.7	>3.7	3.7 ± 0.5
SK3M4M5M	0.12 ± 0.06	0.59 ± 0.34	0.58 ± 0.28	0.75 ± 0.34	16.2 ± 1.8
AG110	2.6 ± 1.4	37.8 ± 3.9	30.7 ± 9.0	81.4 ± 6.6	>100
LZ37	12.1 ± 2.6	>92.6	54.7 ± 11.2	6.2 ± 2.0	92.6 ± 5.4
BPIP	0.22 ± 0.02	>76.5	47.8 ± 40.6	1.1 ± 0.1	76.5 ± 2.2

EC_{50}: 50% effective concentration, based on the inhibition of virus-induced cytopathicity; CC_{50}: 50% cytotoxic concentration, based on the reduction of viable cell number. All data represent means ± SD for three independent experiments.

they share the same target with the nonnucleoside NS5B inhibitors AG110, LZ37, and BPIP. The latter compounds were shown to select for drug resistance mutations in the top of the finger domain of the viral polymerase. Interestingly, γ-carboline, SK4M5M, and SK1M4M5M almost completely lost their activity against the resistant mutants. In contrast, SK3M4M5M retained most of its antiviral activity (EC_{50} < 1.0 μM). The methyl group at the 3-position of γ-carboline may possibly play an important role in retaining the antiviral activity against the resistant mutants as well as enhancing the activity against the wild-type strain.

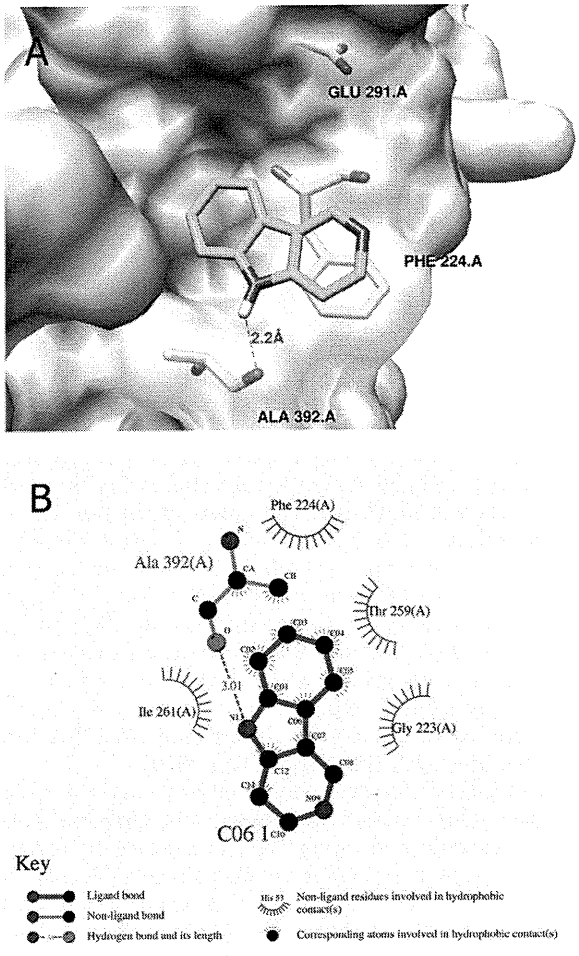

Fig. 5. Modeling of γ-carboline near the position of F224 in BVDV RNA-dependent RNA polymerase. (A) Overview of the entire structure of the RNA polymerase with γ-carboline docked in the vicinity of F224. Picture generated using UCSF Chimera (Pettersen et al., 2004). (B) Ligplot depicting a simplified representation of interactions between γ-carboline and the RNA polymerase. Carbon atoms are black, nitrogen atoms are blue, and oxygen atoms are red. A putative hydrogen bond is drawn as a dotted black line in panel A and a dotted green line in panel B. Spiked red line indicates the hydrophobic interactions.

We hypothesize that the apparent lack of cross-resistance of SK3M4M5M with the drug resistant strains can be explained by a different binding mode of each analogue, as compared to that of γ-carboline; likely due to the different degree of methylation and the position of the methyl groups. For SK3M4M5M, the methyl group in position 3 is optimal to interact with the wild-type RNA polymerase. However, this methyl group will shift the interaction of the molecule, as compared to γ-carboline. Most probably, this shift will result in the loss of the aromatic ring stacking interaction between F224 or Y224 and γ-carboline. Hence, the effect on compound activity may be reduced, when these residues are mutated to non-aromatic residues in the drug-resistant strains.

BVDV is considered to be a valuable surrogate virus for identifying and characterizing anti-HCV compounds. BVDV shares many characteristic similarities with HCV in virion structure, genome organization, and replication machinery (Buckwold et al., 2003; Nam et al., 2001). However, it is not surprising that SK3M4M5M did not have selective anti-HCV activity in HCV RNA replicon cells. A possible explanation is the difference between BVDV NS5B and HCV NS5B molecules. It was recently reported that BPIP, which is inactive against HCV, became active, when one or two fluorine molecules were introduced into certain positions of this compound (Vliegen et al., 2009). Currently, this approach has not been successful for γ-carboline derivatives (data not shown).

In conclusion, our results clearly demonstrate that novel γ-carboline derivatives, especially, 3,4,5-trimethyl-γ-carboline (SK3M4M5M) is a highly potent and selective inhibitor of BVDV replication in cell cultures. Although further studies, such as selection of drug-resistant mutants and inhibition of in vitro transcription, are required, the compound may target NS5B RNA polymerase. It retains sufficient activity against the mutant viruses that are resistant to already known nonnucleoside NS5B inhibitors. Thus, this class of compounds should be further pursued for their use in the field of veterinary medicine.

Acknowledgments

This work was in part supported by the Science and Technology Incubation Program in Advanced Regions, Japan Science and Technology Agency (JST), Japan. We thank the Egyptian Government for support to M.T.A. Salim, who was previously an assistant lecturer in the Faculty of Pharmacy, Al-Azhar University, Egypt and is currently a postgraduate student of Kagoshima University, Japan.

References

Aoyama, H., Sako, K., Sato, S., Nakamura, M., Miyachi, H., Goto, Y., Olamoto, M., Baba, M., Hashimoto, Y., 2009. Polymethylated γ-carbolines with potent anti-bovine viral diarrhea virus (BVDV) activity. Heterocycles 77, 779–785.

Baba, C., Yanagida, K., Kanzaki, T., Baba, M., 2005. Colorimetric lactate dehydrogenase (LDH) assay for evaluation of antiviral activity against bovine viral diarrhea virus (BVDV) in vitro. Antiviral Chem. Chemother. 16, 33–39.